energies

MDPI

Review

A Comprehensive Review on the Recent Development of Ammonia as a Renewable Energy Carrier

Muhammad Heikal Hasan [1,*], Teuku Meurah Indra Mahlia [1,*], M. Mofijur [1], I.M. Rizwanul Fattah [1], Fitri Handayani [2], Hwai Chyuan Ong [1] and A. S. Silitonga [3]

[1] Centre for Green Technology, Faculty of Engineering and IT, University of Technology Sydney, Sydney, NSW 2007, Australia; MdMofijur.Rahman@uts.edu.au (M.M.); IslamMdRizwanul.Fattah@uts.edu.au (I.M.R.F.); HwaiChyuan.Ong@uts.edu.au (H.C.O.)
[2] Department of Mechanical Engineering, Syiah Kuala University, Banda Aceh 23111, Indonesia; fitri.mech@gmail.com
[3] Department of Mechanical Engineering, Politeknik Negeri Medan, Medan 20155, Indonesia; ardinsu@yahoo.co.id
* Correspondence: muhammadheikal.hasan@student.uts.edu.au (M.H.H.); TMIndra.Mahlia@uts.edu.au (T.M.I.M.); Tel.: +61-4123-08541 (M.H.H.); +61-2951-490571 (T.M.I.M.)

Abstract: Global energy sources are being transformed from hydrocarbon-based energy sources to renewable and carbon-free energy sources such as wind, solar and hydrogen. The biggest challenge with hydrogen as a renewable energy carrier is the storage and delivery system's complexity. Therefore, other media such as ammonia for indirect storage are now being considered. Research has shown that at reasonable pressures, ammonia is easily contained as a liquid. In this form, energy density is approximately half of that of gasoline and ten times more than batteries. Ammonia can provide effective storage of renewable energy through its existing storage and distribution network. In this article, we aimed to analyse the previous studies and the current research on the preparation of ammonia as a next-generation renewable energy carrier. The study focuses on technical advances emerging in ammonia synthesis technologies, such as photocatalysis, electrocatalysis and plasmacatalysis. Ammonia is now also strongly regarded as fuel in the transport, industrial and power sectors and is relatively more versatile in reducing CO_2 emissions. Therefore, the utilisation of ammonia as a renewable energy carrier plays a significant role in reducing GHG emissions. Finally, the simplicity of ammonia processing, transport and use makes it an appealing choice for the link between the development of renewable energy and demand.

Keywords: ammonia; renewable energy storage; hydrogen storage

Citation: Hasan, M.H.; Mahlia, T.M.I.; Mofijur, M.; Rizwanul Fattah, I.M.; Handayani, F.; Ong, H.C.; Silitonga, A.S. A Comprehensive Review on the Recent Development of Ammonia as a Renewable Energy Carrier. *Energies* **2021**, *14*, 3732. https://doi.org/10.3390/en14133732

Academic Editor: Rob J.M. Bastiaans

Received: 30 April 2021
Accepted: 16 June 2021
Published: 22 June 2021

1. Introduction

Industrial activity in parts of the world often has several direct and indirect adverse environmental consequences. Carbon dioxide (CO_2), a natural greenhouse gas (GHG) that helps keep the globe warm, is out of control and triggering a climate crisis. This anthropogenic emission endangers human health, agriculture, natural ecosystems and atmospheric stability [1]. As reported in the Intergovernmental Panel on Climate Change (IPCC) Climate Change Mitigation Report (2014), CO_2 is the main contributor to GHG emissions, which have 76% (including 11% of forests and land use) of the overall share, while CH_4 and N_2O accounted for 16% and 6%, respectively [2]. According to National Oceanic and Atmospheric Administration (NOAA), global ambient CO_2 concentrations rose from 280 ppm to 407.4 ppm in 2018, setting a new high for the last 800,000 years [3,4].

A growing number of international reports illustrates the health and environmental effects of GHG emissions [5–7]. The ultimate goal is to maintain GHG concentrations at a point where the dangerous effect of climate change can be prevented. In 1997, the convention was supplemented and updated by the Kyoto Protocol [8]. Unlike the United

Nations Framework Convention on Climate Change (UNFCCC), the Kyoto Protocol binds parties from a developed country to reduce GHG emissions [9]. Recently, under the terms of the Paris Agreement of 2015, the United Nations (UN) has committed itself to a long-term target to keep temperatures below 2 °C, compared to pre-industrial levels, to avoid the worst consequences of global warming [10,11]. Figure 1 shows the top 10 countries on CO_2 emissions worldwide and their goal in the Paris Agreement.

In the last decades, the world has put great effort and investment into developing renewable energy to decarbonise the economy. The global pandemic disruption caused by COVID-19 teaches humanity that reducing the proportion of fossil fuels in human activity will substantially increase the regeneration of the Earth's atmosphere due to a reduction in air pollution. For example, in China, restricting the activity of people caused by the COVID-19 pandemic resulted in a 25% and 50% reduction in CO_2 and NO_X emissions, respectively [12,13]. However, the problem with these renewable sources of energy is that they are highly weather-dependent. Therefore, it is necessary to have an affordable and efficient method for storing energy. Several prevailing storage technologies, such as chemical, mechanical, electrical and thermal energy storages, can be applied from small to large-scale applications. Prominent storage solutions, such as batteries, provide durability and technological sophistication but are far too expensive and cannot provide the power needed for seasonal and grid-scale demand. Consequently, hydrogen has been the best candidate since the 1970s, positioning this as both energy storage and a clean energy source [14]. However, storage and delivery issues associated with H_2 remain an obstacle to its implementation [15]. To store and distribute H_2 efficiently, other indirect storage media such as ammonia (NH_3), with its proven transportability and high flexibility, is required [16].

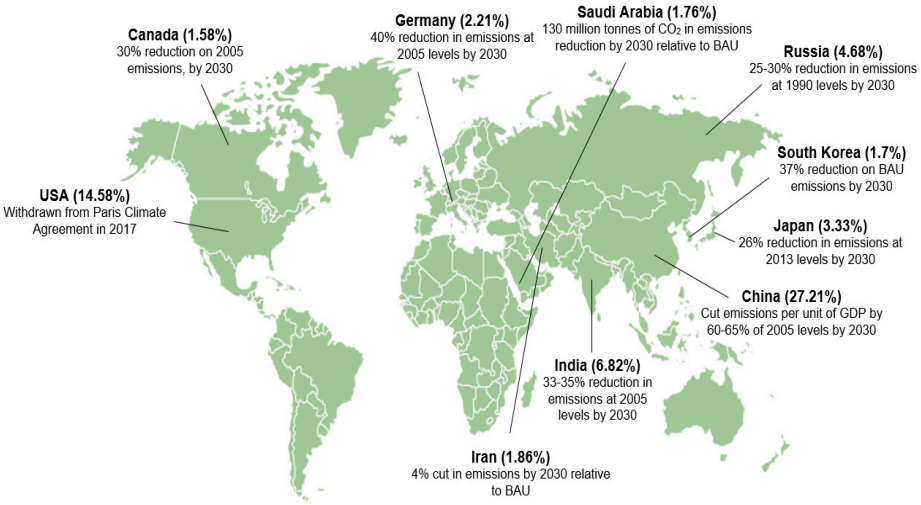

Figure 1. Top 10 global CO_2 emitters and the target in the Paris Agreement [17].

In some countries, ammonia has become a part of their energy roadmap. For example, Japan's Cross-Ministerial Strategic Innovation Program (SIP) attempts to show ammonia, hydrides and hydrogen as essential elements of the nation's hydrogen energy system [18]. The Japanese Ministry of Economy, Trade and Industry (METI) described ammonia in conjunction with "the concept of importing renewable energy produced in other countries" [19]. In the United States, The Advanced Research Projects Agency-Energy (ARPA-E) announced a cumulative grant of $32.7 million for 16 projects, 13 of which focus on ammonia [16]. Governments in New Zealand and Australia have announced federal grants to support the development of ammonia plants driven by renewable energy. More recently, Australia has awarded Yara and ENGIE AU$995,000 for their solar ammonia project, Yara Pilbara, from the Australian Renewable Energy Agency (ARENA). As for New Zealand, Ballance-Agri Nutrients and Hiringa Energy received NZ$19.9 million from

the Provincial Growth Fund for their wind-fed ammonia plant in Kapuni [20]. Similarly to Japan, the country is also looking into the possibility of exporting renewable energy in the form of ammonia. In addition, Toyota and Commonwealth Scientific and Industrial Research Organization (CSIRO) designed the first ammonia fuel car tested in Australia in 2018 [21].

Today, with a global production rate of more than 176 million metric tonnes of ammonia, the chemical is being used as fertiliser and a building block in the manufacture of many products [22,23]. With 28.5% of global production, China is known as the main producer of ammonia [24]. The uses of ammonia as an intermediate for the production of fertilisers account for over 80% of the total production of ammonia [25]. Other applications include fibre and plastics, pharmaceuticals, mining and metallurgy, pulp and paper, refrigeration and explosives [26]. Other than that, ammonia has also being recently proposed to be used in automotive applications for NOx emission control (DeNOx) technologies [27]. Furthermore, ammonia has also been researched as a source of energy for fuel cells, transport, industry and power generation [28].

Unfortunately, the current industrial ammonia synthesis method is complicated, energy-intensive and heavily dependent on hydrocarbon. The Haber–Bosch process that is currently used to synthesise ammonia is responsible for almost 11% of global industrial CO_2 emissions [29,30]. In addition, the nature of renewable energy sources, which are irregular, requires turnkey systems that can be instantly switched on and off [31]. Thus, the challenge for the global deployment of ammonia as energy storage is, therefore, the simpler and more efficient production of ammonia from abundant sources, such as ambient air and water, with a ready to go system, which can be driven by intermittent energy sources.

The number of research studies on renewable ammonia, its innovation on the production route and its performances as a fuel has increased substantially in recent years, as shown by a growing number of scientific papers and review papers (Figure 2a–c). There has been a significant increase in the numbers of scientific articles related to ammonia, renewable energy, energy storage or energy carriers in recent years. For innovative approaches of ammonia synthesis, electrochemistry gained great attention in recent years due to the direct conversion of electricity into ammonia. Of all the devices capable of converting ammonia into energy, the Internal Combustion (IC) engine appears to receive the most development effort, noting that use for other applications is less explored.

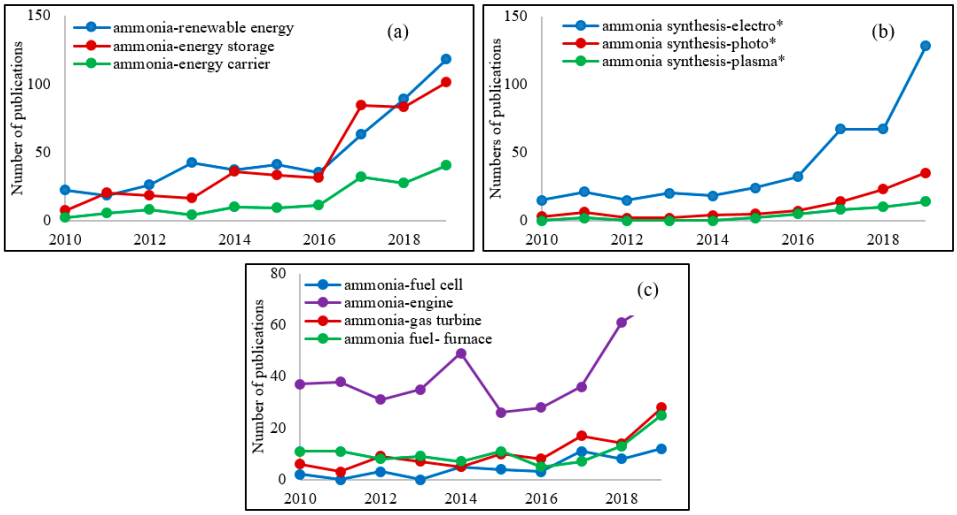

Figure 2. Recent publications of (**a**) ammonia as a renewable energy carrier, (**b**) innovations in ammonia production, (**c**) ammonia as a fuel in Scopus databases.

This study comprehensively reviews all aspects of ammonia as energy storage, including innovative approaches for converting renewable energy into ammonia and devices that

convert ammonia into energy. The comparison of the recent review article of ammonia as renewable energy and this work is given in Table 1.

Table 1. The comparison of recent review articles on ammonia as a renewable energy carrier and this work.

Category	[16]	[32]	[33]	[34]	[35]	[36]	[37]	This Work
Ammonia economy	√	-	-	-	√	-	√	√
Photocatalysis	-	-	-	-	-	-	-	√
Electrocatalysis	-	√	√	√	-	√	-	√
Plasmacatalysis	-	-	√	-	-	√	-	√
Fuel cell	√	-	-	-	√	-	√	√
IC engine	√	-	-	-	√	-	-	√
Gas turbine	√	-	-	-	√	-	-	√

2. Key-Driver of Ammonia Economy

The issue of the storage and distribution of hydrogen creates opportunities for ammonia to be seen as alternative storage of renewable energy. The previous study on the potential hydrogen storage material by Kojima [38] has revealed that ammonia has the highest gravimetric densities with the highest volumetric densities, as shown in Figure 3 [16,38]. Consequently, attempts are being made to leverage ammonia over others to replace hydrogen as a central energy distribution block [16]. In addition, ammonia can be used to replenish soil nutrients, boosting the growth of crops and accelerating afforestation that will indirectly help to balance CO_2 gas in the atmosphere through photosynthesis by plants.

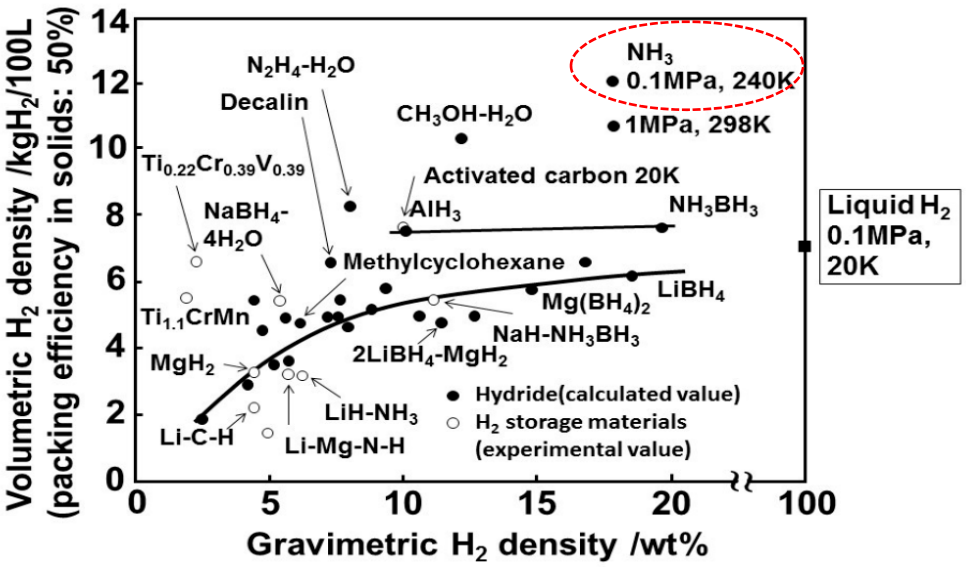

Figure 3. The density of hydrogen in hydrogen carriers [38].

The sustainable future of renewable energy-driven ammonia production is not a novel idea but has never been widely embraced over methane or coal-based ammonia. By transforming into ammonia that can be liquefied under moderate pressure, renewable energy can be transported from places where renewable energy is cheap or excessive to where it is limited or expensive. This synergy could open up opportunities for exports and imports of renewable energy, similar to today's hydrocarbon fuel. In addition to being used directly in the form of ammonia, this may also be dissociated into its component for use as hydrogen fuel at a relatively low cost. Cost comparison of the hydrogen produced from a variety of feedstock is presented in Table 2.

Table 2. Cost comparison of hydrogen production via various feedstock [39–43].

Method	Electricity Source	Hydrogen Production (kg/day)	Hydrogen Cost ($/kg)
Water electrolysis	Wind	1400–62,950	5.10–23.37
	Solar PV	1356	10.49
	Solar Thermal	1000	7.00
	Nuclear	1000	4.15
Thermochemical water splitting	Solar	6000	7.98–8.40
	Nuclear	7000–800,000	2.17–2.63
Natural Gas steam reforming	With carbon capture storage	-	2.27
	Without carbon capture storage	-	2.08
Coal gasification	With carbon capture storage	-	1.63
	Without carbon capture storage	-	1.34
Biomass gasification	-	-	1.77–2.05

In addition to the aforementioned factors, ammonia transportation and storage facilities already exist today, where around 18 million tonnes of ammonia are exchanged annually. Unlike hydrogen that cannot be liquefied under a pressurised tank, ammonia may be kept in liquid form when at least 8.58 bar is maintained. Under this load, carbon steel tanks are sufficient to be used. Ammonia may also be contained as a liquid in lower temperature storage if the temperature of −33 °C is preserved while hydrogen only can be liquefied under cryogenic cooling at −252.87 °C. The energy density in this form is roughly half that of petrol and more than ten times that of batteries. Ammonia also offers a much lower storage cost compared to hydrogen. Commonly, long-distance ammonia transport is accomplished by using carbon steel pipelines that are opposed to hydrogen, which now still has material issues with the pipeline. For transporting ammonia via pipeline over 1610 km, it requires 1119 kJ/kg-H_2, which is much lower than that of hydrogen transport of 14,814 kJ/kg-H_2. This disparity can be described by the state of the two fluids where hydrogen gas is distributed with the aid of compressors while the ammonia is carried as a liquid using a pump. The comparison between ammonia and hydrogen is given in Table 3.

Table 3. Difference between NH_3 and H_2 in terms of storage and distribution [39,44,45].

Parameter	Ammonia	Hydrogen	Hydrogen
Storage method	Liquid	Compressed	Liquid
Storage pressure (MPa)	1.1	70	-
Liquefy temperature (°C)	−33	-	−252.87
Fuel density (kg m^{-3})	600	39.1	70.99
Storage cost over 182 days ($/kg-$H_2$)	0.54	-	14.95
Transporting over 1610 km pipeline (kJ/kg-H_2)	1119	14,814	-

Ammonia also can be transported as a pressurised liquid via truck and rail. Trailers can transport 43,530 L ammonia at 2.07 MPa. Such a tank could hold up to 26 tonnes or 600 GJ of energy of ammonia [46]. In contrast, a hydrogen lorry only can be used to transport around 340 kg of hydrogen gas at 17.91 MPa, equivalent to 48 GJ of hydrogen energy content, while transporting in liquid form in a hydrogen trailer could hold around 3.9 tonnes of hydrogen, equal to 553 GJ of energy [47]. Rail transport uses a pressurised tank with a capacity of 126,810 L at 1.55 MPa, which indicates the capability to carry 77.5 tonnes of NH_3 [46]. Ammonia can be transported by ship or barge using pressurised storage vessels. By using these vessels, existing ocean-going ships can transport 55,000 tonnes of ammonia [48]. The NH_3 and H_2 transport methods are summarised in Table 4.

Table 4. Differences in NH_3 and H_2 transport methods [44].

Parameter	Ammonia			Hydrogen	
	Truck	**Rail**	**Ship**	**Truck**	**Truck**
Storage method	Liquid	Liquid	Liquid	Compressed	Liquid
Storage pressure (MPa)	2.07	1.55	-	17.91	-
Capacity (tonnes)	26	77.5	55,000	0.34	3.9
Energy capacity (GJ-HHV)	600	1746	1,240,000	48	553

Note: HHV (higher heating value).

In the recent development, storing ammonia as metal ammine complexes, i.e., hexaamminemagnesium chloride, $Mg(NH_3)_6Cl_2$ (Figure 4), also gives a beneficial advantage for storing and transporting since it has very low vapour pressure (0.002 bar at ambient temperature) [49,50]. Hexaamminemagnesium chloride is formed simply bypassing ammonia at room temperature over anhydrous magnesium chloride. $Mg(NH_3)_6Cl_2$ can be formed into a small and dense solid without any void space. The amine has volumetric hydrogen content between 105 and 110 kg H_2 m^{-3} and gravimetric hydrogen content over 9 wt.% [49].

Figure 4. $Mg(NH_3)_6Cl_{l2}$ for ammonia storage [50].

3. Ammonia-Based Energy Storage

3.1. Characteristics

Ammonia is comprised of N_2 and H_2 with the chemical formula of NH_3. A highly irritating, colourless gas with a distinctive pungent scent characterises the chemical. With a density of 0.769 kg m^{-3}, ammonia is lighter than air. It also liquefies easily, which is caused by a resilient hydrogen bond among molecules. The boiling point and the freezing point at standard temperature and pressure are −33.35 °C and −77.65 °C, respectively. Ammonia in the air has a flammability limit between 15 and 25%. Ammonia burns with a light yellowish-green flame. Where a suitable catalyst and high temperature is present, ammonia is decomposed into the constituent elements.

The ammonia molecule has a pyramidal trigonal form with an angle of the bond of 106.7 °C. The atom of nitrogen consists of five outer electrons with an additional three electrons from each hydrogen atom, giving eight electrons in total, or pairs of four tetrahedral arranged electrons. This shape gives a dipole moment to the molecule, which makes it polar. The polarity of the molecule and, in particular, its capability to create hydrogen bonds makes ammonia very soluble in water. The chemical is naturally a base and a

proton acceptor. Ammonia aqueous solution with a concentration 1.0 M has a pH of 11.6 at 298 K [51]. Even though accidental explosion or combustion is relatively low [16], the US-National Fire Protection Association (NFPA) has identified this as a hazardous material, putting it at high safety risk [52]. Safety concerns regarding ammonia storage for end-users arise due to the high vapour pressure of liquid ammonia. At high temperatures, ammonia can decompose, forming highly flammable hydrogen and toxic nitrogen oxide. Ammonia is also known to be corrosive with certain alloys such as copper, brass and bronze, as presented in Table 5.

Table 5. Material compatibility of ammonia and its derivative [16,53–55].

Materials	Ammonium Hydroxide (Ammonia in Water)	Ammonia Anhydrous
ABS plastic	-	D
Acetal (Delrin ®)	D	D
Aluminium	C	A
Brass	-	D
Bronze	-	D
Buna N (Nitrile)	D	B
Carbon graphite	-	A
Carbon steel	D	B
Carpenter 20	-	A
Cast iron	D	A
ChemRaz (FFKM)	-	B
Cooper	-	D
CPVC	-	A
EPDM	A	A
Epoxy	-	A
Fluorocarbon (FKM)	B	D
Hastelloy-C ®	B	B
Hypalon ®	A	D
Hytrel ®	-	D
Kalrez	-	A
Kel-F ®	-	A
LDPE	-	B
Leather		D
Natural rubber	-	D
Neoprene	B	A
NORYL ®	-	B
Nylon	C	A
Polycarbonate	-	D
PEEK	-	A
Polypropylene	A	A
Polyurethane	-	D
PPS (Ryton ®)	-	A
PTFE	A	A
PVC	-	A
PVDF (Kynar ®)	A	A
Santropene	A	A
Silicone	-	C
Stainless Steel 304	B	A
Stainless Steel 316	A	A
Titanium	-	C
Tygon ®	-	A
Viton ®	-	D

Note: A (excellent); B (good); C (fair); D (poor).

Ammonia is also fatal if inhaled, causing a lung injury. Some people may be somewhat irritated by 30 ppm for 10 min, while the remainder is sensitive to 50 ppm. At 500 ppm, the nose and throat get immediate and severe irritation. Short exposure to levels over

1500 ppm can lead to fluid accumulation in the lungs [56]. Immediately Dangerous to Life and Health (IDLH) is the degree whereby a healthy person can get 30 min of exposure without causing permanent health effects. Ammonia is also believed to be responsible for the depletion of ozone by an accumulation of nitrous compounds in the atmosphere [57]. Table 6 summarises the Health and Safety data, including their vapour pressure, IDLH and toxicity.

Table 6. Health and Safety data of ammonia and its derivatives [58–60].

Carriers	VP at 20 °C (Bar)	IDLH (ppm)	AT 20 °C ($IDLH^{-1}$)
35 wt.% NH_3 solution	1.24	-	~4133
NH_3 (liquid)	8	300	~27,000
$Mg(NH_3)_6Cl_2$	1.4×10^{-3}	-	4.65

Note: VP (vapour pressure); AT (apparent toxicity).

3.2. Ammonia production Using Haber–Bosch Method

Fritz Haber and Carl Bosch invented the Haber–Bosch (H–B) process in the middle of the 20th century, replacing the Birkeland–Eyde process and Frank–Caro process to synthesise ammonia [37]. Since its discovery, the Haber–Bosch process dominating the industrial process and has undergone many substantial improvements and optimisations. The minimum energy consumption in the mid-1950s is reduced from more than 60 GJ $t_{NH3}{}^{-1}$ to 27.4–31.8 GJ $t_{NH3}{}^{-1}$ today [61]. Such improvements represent an improvement in overall energy efficiency from 36 to 65%. The most significant increase in productivity was made by replacing coal with CH_4 to produce H_2.

In short, the production cycle of ammonia can be broken down into two major phases; the first is synthetic mixture production, and the subsequent is the synthesis of ammonia synthesis by the H–B process. In the first phase, hydrogen production takes place via two-stage steam methane reforming (SMR) reactors before being transferred for water-gas-shifting (WGS) reaction, CO_2 subtraction and then methanation [61]. The primary SMR reactor works at 850–900 °C and 25–35 bar that travels through the catalyst. In this process, the energy needed for the endothermal reactions generated by the external combustion of methane fuel through the furnace [61]. Water-saturated methane is then fed into a catalytic converter that converts methane to hydrogen and carbon monoxide before it is transferred to a second SMR. In the secondary SMR, ambient air is compressed and transferred at 900–1000 °C to partially oxidise reagents in the next reactor. In this process, air–oxygen and steam convert unreacted methane into hydrogen and carbon monoxide, besides providing the stoichiometric nitrogen required for Haber–Bosch downstream reactions [58].

The next process involves converting carbon monoxide to carbon dioxide by steam injection in the WGS reactor to prevent coke from forming on the catalyst and side reactions. The feed is then sent to a CO_2 remover column, giving a nitrogen and hydrogen-rich feed with high purity for the next process [61]. The ammonia production then takes place on Haber–Bosch reactor when the process is usually performed in a reactor with two to four catalytic converter beds at 200 to 350 bar and 300 to 500 °C [58]. Since the process has low single-pass conversion efficiency (~15%), it is necessary to recycle the unreacted gas. The nitrogen fixation process for ammonia and the reaction process that occurs during the Haber–Bosch process is shown below:

$$N_2 + 3H_2 \rightarrow 2NH_3 \; \Delta H_{298K} = -92 \text{ kJ mol}^{-1} \quad (1)$$

$$CH_4 + H_2O \rightarrow CO + 3H_2 \text{ (Primary Steam Reforming)} \quad (2)$$

$$4CH_4 + O_2 + 2H_2O \rightarrow 10H_2 + 4CO \text{ (Secondary Steam Reforming)} \quad (3)$$

$$CO + H_2O \rightarrow CO_2 + H_2 \text{ (Water} - \text{gas shift)} \quad (4)$$

3.3. Electrically-Driven Haber–Bosch Process

Notwithstanding the technological reliability of the existing Haber–Bosch process, the question remains as to whether or not such a process can be CO_2-free. To answer these questions, research and development are underway worldwide to substitute the centuries-old Haber–Bosch method for the production of ammonia, driven by renewable electricity. It includes switching H_2 obtained from the steam-reformed CH_4 to H_2 obtained from the electrolysed H_2O. Given the trend in renewable energy prices to compete with fossil fuels, the green Haber–Bosch process is no longer a vision. Figure 5 shows the electrically driven Haber–Bosch plant powered by renewable energy.

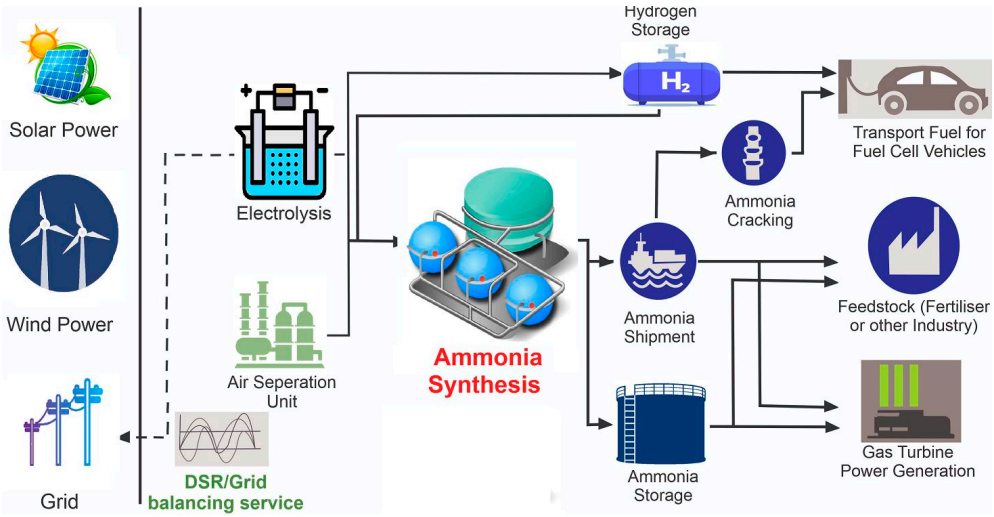

Figure 5. Schematic of renewable energy-driven Haber–Bosch plant [62].

Ammonia synthesis processes powered by renewable energy have been demonstrated in many countries. For example, in the USA, Schmuecker Pinehurst Farm LLC has built a solar ammonia plant and has been in operation for many years where H_2 and N_2 are generated from water and air by electrolysis and power swing system before pressurised and fed into the ammonia production facility [63]. In Zimbabwe, Africa, an ammonium nitrate plant was developed where ammonia is supplied from renewable energy-driven Haber–Bosch process. This production facility has been productive for years, with 240,000 tonnes of ammonium nitrate produced annually [64]. In Australia, several projects have been developed near Yara Pilbara, Western Australia [65] and Port Lincoln, South Australia [66] to evaluate the feasibility of renewable energy-driven ammonia plants. At the same time as optimisation of the renewable energy-driven Haber–Bosch process, the development of alternative methods to allow the N_2 reduction reaction at atmospheric pressure and moderate ambient temperature, such as photocatalysis, electrocatalysis and plasmacatalysis has attracted widespread interest in ammonia synthesis today.

4. Innovative Approaches for Ammonia Synthesis

In the absence of high temperatures and pressures, nature converts molecular N_2 to NH_3. This natural process uses enzyme nitrogenises containing metal ions (iron and molybdenum) to induce ammonia reactions from atmospheric nitrogen, electrons and protons. This phenomenon has aroused the researcher's interest in imitating nature.

In recent times, significant progress in understanding the process for nitrogenises reactions and in creating a modern synthetic method has been achieved. Photocatalysis, plasmacatalysis and electrocatalysis have been studied as alternative green routes for ammonia production. These new techniques offer distinct advantages compared to the old Haber–Bosch method.

Among those, the plasma-enabled ammonia synthesis is both energy and cost-effective in theory. The potential energy consumption of non-thermal plasma (NTP) ammonia

production has been reported to be around 0.2 MJ/mol, which is lower than the Haber–Bosch technique (0.48 MJ/mol) [67]. This section details the method and provides a discussion on emerging technology for facilitating the N_2 reduction reaction to ammonia.

4.1. Photocatalysis

Photocatalytic ammonia production from water and air at low temperature and pressure show enormous potential, attracting increased research interest from scientists. The process is relatively safe, inexpensive and accessible to a free energy source (light). In general, photons are used in the photocatalytic mechanism to drive N_2 activation. The fixation process of N_2 into NH_3 by photocatalysts can be represented by the following equation:

$$N_2 + 3H_2O \xrightarrow{\text{light}} 2NH_3 + \frac{3}{2}O_2 \quad (5)$$

The N_2 fixation photocatalytic process involves several steps. In short, the electron generated by the photocatalyst effect is driven into the conduction band, creating an empty hole in the valance band. Some holes and electrons are then recombined together, while others transfer to the catalytic surface and take part in the redox reaction. H_2O is then oxidised to O_2 by holes, while N_2 is reduced to NH_3 by the reaction of water-derived protons and photo-generated electrons. Figure 6 illustrated the catalytic process of the photocatalyst.

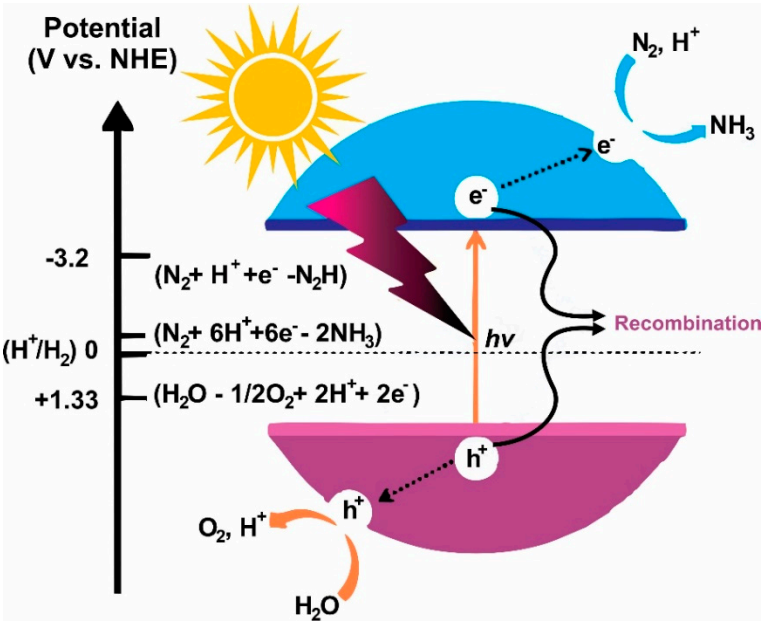

Figure 6. Schematic of photocatalyst reaction for ammonia synthesis [68].

TiO_2-based metal oxide photocatalysts were studied early in nitrogen fixation because of less expense and higher stability. Following the pioneering research in 1977 by Schrauzer and Guth [69], many semiconductors have been proposed for the process of photocatalysis viz. metal oxide, metal sulphide, oxyhalides and other graphitic nitride carbon materials.

In 1988, Bourgeois et al. [70] studied photocatalytic action of unmodified TiO_2 after annealing under atmospheric air pressure. Thermal pre-treatment is believed to trigger surface defects that caused defects or impurities in the semiconductor bandgap. In the most recent study, the photocatalytic N_2 fixation into NH_3 on TiO_2 surface oxygen vacancies was systematically investigated by Hirakawa et al. [71]. They found that the active sites for N_2 reduction are the oxygen vacancies of the Ti^{3+} species. The superficial Ti^{3+} provided an abundance of active N_2 fixing sites by acting as an electron donor, resulting in relatively easy dissociation of the N≡N bond. In other studies, many other metal species are used as

doping in the TiO_2 catalyst; however, the photocatalytic was unsatisfactory. The transition metal atoms loaded into TiO_2 can function as co-catalysts while acting as a dopant in the TiO_2 matrix. In addition, the Schottky junction formation on the semiconductor interface and the transition metal induces electrical fields and facilitates the separation of photo-induced electrons and holes.

In addition to metal doping, noble metals may also be embedded onto the surface of TiO_2. Ranjit et al. [72], in 1996, compared four noble metals (Ru, Rh, Pd, Pt) as TiO_2 co-catalysts. They found Ru > Rh > Pd > Pt to be the order of photoactivity between metals, which is closely related to the strength of the noble metals and the hydrogen bond. The experiment revealed that noble metals with higher barriers to H_2 evolution exhibit surprisingly higher NH_3 yields.

The development of metal-doped TiO_2 in N_2 fixation sparked interest in the development of binary metal oxide and ternary metal oxides as doping. The study by Lashgari and Zeinalkhani [73], on the synthesis of Fe_2O_3 by precipitation method, found that the ammonia is efficiently formed from N_2 at Fe_2O_3 nanoparticles. It was also reported that partially reduced Fe_2O_3 may be used for the reduction of photocatalytic N_2. More recently, bismuth monoxide (BiO) was employed for N_2 photoreduction. It has been stated that BiO quantum dots will significantly decrease N_2 at 1226 μmol $gcat^{-1}h^{-1}$ NH_3 with the simulated rate of sunlight [74].

In addition to metal oxides, the study of metal sulphides in the field of photocatalysis has also seen a significant increase in the scientific community. The metal sulphide band gap is conducive to intense visible light absorption, resulting in highly effective solar use. As a result of the growing multidisciplinary research in biology and material science, organic-sulphide has also been developed as a catalyst for NH_3 synthesis [68]. Researchers questioned whether sulphur vacancies could effectively promote the photocatalytic event. Motivated by this idea, Hu et al. [75] studied the sulphur vacancies effect on the efficiency of ternary metal sulphide for N_2 fixation. Sulphur vacancies have been found to introduce surface chemical adsorption sites, which have helped to activate N_2 molecules by widening the bonding space from 1.164 Å to 1.213 Å. In the recent development, $Cd_{0.5}Zn_{0.5}S$ solid solution loaded with Ni_2P was effectively reduced N_2 with the NH^3 yield of 253.8 μmol $g_{cat}{}^{-1}$ h^{-1} [76]. Other materials, such as Bismuth oxyhalides, are also found to be promising photocatalysts due to their layered crystal structure and suitable band gaps [68,77].

Other than the material mentioned above, graphitic nitride carbon photocatalyst for N_2 fixation has been designed and developed in recent years. Dong et al. [78] have shown that introducing vacancies in nitrogen will dramatically boost the photocatalytic behaviour of g-C_3N_4. It was because the nitrogen vacancies, which had the size and forms as the nitrogen atoms, are advantageous for adsorbing and activating the chemically inert N_2. In another study, honeycombed g-C_3N_4 doped with Fe^{3+} has shown enhanced photocatalytic performance [79]. After that, various forms of photocatalysts based on g-C_3N_4 were employed in photochemical ammonia synthesis. A summary of various photochemical catalysts by previous studies is presented in Table 7.

Table 7. Recent studies on photochemical catalysis systems for ammonia production.

Groups	Catalyst	T (K)	Scavenger	Catalyst Loading ($g\ L^{-1}$)	NH_3 Yield ($\mu mol g_{cat}{}^{-1}h^{-1}$)	Ref
Metal oxides	TiO_2	500	-	-	0.83	[70]
	0.4 wt.% Co-doped TiO_2	313	-	-	6.3	[69]
	0.4 wt% Cr-doped TiO_2	313	-	-	0.37	[69]
	0.4 wt% Mo-doped TiO_2	313	-	-	6.7	[69]
	2 wt% Mg-doped TiO_2	-	-	0.67	6.9 μM h^{-1}	[80]
	0.5 wt% Fe-doped TiO_2	353	-	-	6	[81]
	10 wt% Ce-doped TiO_2	-	-	0.8	3.4 μM h^{-1}	[82]
	10 wt% V-doped TiO_2	-	-	0.8	4.9 μM h^{-1}	[82]

Table 7. *Cont.*

Groups	Catalyst	T (K)	Scavenger	Catalyst Loading ($g\ L^{-1}$)	NH_3 Yield ($\mu molg_{cat}^{-1}h^{-1}$)	Ref
	0.24 wt% Ru-loaded TiO_2	-	-	-	17.3	[72]
	0.8 wt% Pt-loaded TiO_2	-	-	-	4.8	[72]
	0.69 wt% Pd-loaded TiO_2	-	-	-	11.8	[72]
	0.2 wt% Rh-loaded TiO_2	-	-	-	12.6	[72]
	0.2 wt% Fe-doped TiO_2	313	-	-	10	[69]
	Fe-doped TiO_2	298	Ethanol	1	400 $\mu M\ h^{-1}$	[83]
	JRC-TIO-6 (rutile)	313	2-PrOH	1	2.5 $\mu M\ h^{-1}$	[71]
	Pt-loaded ZnO	-	Na-EDTA	-	860	[84]
	Fe_2O_3	298	Ethanol	0.5	1362.5 $\mu M\ h^{-1}$	[73]
	Partially reduced Fe_2O_3	303	-	-	10	[85]
	BiO quantum dots	298	-	-	1226	[74]
	H-Bi_2MoO_6	-	-	-	10	[86]
Metal sulphides	$Zn_{0.1}Sn_{0.1}Cd_{0.8}S$	303	Ethanol	0.4	105.2 $\mu M\ h^{-1}$	[75]
	CdS/Pt	311	-	-	3.26	[87]
	CdS/Pt/RuO_2		-	4	620 $\mu M\ h^{-1}$	[88]
	MoS_2	298	-	-	325	[89]
	$Mo_{0.1}Ni_{0.1}Cd_{0.8}S$	303	Ethanol	0.4	71.2 $\mu M\ h^{-1}$	[90]
	g-C_3N_4/ZnMoCdS	298	Ethanol	0.4	77.6 $\mu M\ h^{-1}$	[91]
	g-C_3N_4/ZnSnCdS	303	Ethanol	0.4	167.6 $\mu M\ h^{-1}$	[92]
	$Ni_2P/Cd_{0.5}Zn_{0.5}S$	293	-	-	253.8	[76]
Oxyhalides	Bi_5O_7I	293	Methanol	0.5	111.5 $\mu M\ h^{-1}$	[93]
	BiOCl	298	Methanol	0.67	46.2 $\mu M\ h^{-1}$	[94]
	BiOBr	298	-	0.5	1042 $\mu M\ h^{-1}$	[95]
	Bi_5O_7Br nanotubes	-	-	-	1380	[96]
Graphitic nitride carbon	Fe-doped g-C_3N_4	303	Ethanol	0.4	120 $\mu M\ h^{-1}$	[79]
	g-C_3N_4	-	Methanol	1	160 $\mu M\ h^{-1}$	[78]
	g-C_3N_4/MgAlFeO	303	Ethanol	0.4	166.8 $\mu M\ h^{-1}$	[97]
	g-C_3N_4/rGO	303	Na-EDTA	0.4	206 $\mu M\ h^{-1}$	[98]
	Ga_2O_3-DBD/g-C_3N_4	-	Ethanol	0.4	112.5 $\mu M\ h^{-1}$	[99]
	$W_{18}O_{49}$/g-C_3N_4	-	Ethanol	0.4	57.8 $\mu M\ h^{-1}$	[100]

4.2. Electrocatalysis

In addition to photocatalysis, the synthesis of ammonia by the electrocatalysis process is also currently being explored. In a traditional proton-conductive electrolyte cell, gaseous H_2 passes through the anode where it is changed to protons (H^+) while the nitrogen reduction reaction occurs at the cathode [101]. The H^+ then diffuses into the cathode, where it forms NH_3 in combination with the dissociated N. The following equations can describe the reaction:

$$3H_2 \rightarrow 6H^+ + 6e^- \quad (6)$$

$$N_2 + 6H^+ + 6e^- \rightarrow 2NH_3 \quad (7)$$

$$N_2 + 3H_2 \rightarrow 2NH_3 \quad (8)$$

The problem, though, is such cell configuration had to work at low temperatures where the kinetics of reaction were sluggish [102]. Moreover, an electrochemical cell is more advantageous when operating at higher temperatures since higher rates of reaction can be achieved in the same electrode area, and hydrazine development can be prevented [103]. As a result, proton (H^+) conductivity solid-state materials that operate at a temperature above 500 °C were developed [102].

Based on the working temperature, electrocatalytic ammonia synthesis can be broken down into high (higher than 500 °C), intermediate (between 100 °C and 500 °C) and low (lower than 100 °C) [36]. In the high-temperature electrocatalysis process, most of the studies occupy solid electrolytes with perovskite as the material in reactor configuration.

Among the studies, quite high ammonia rates were reported by Wang et al. [104,105] using doped Ceria-$Ca_3(PO_4)_2$-K_3PO_4 composite electrolyte in combination with a Ag-Pd electrode. Ammonia yields up to 9.5×10^{-9} mol $s^{-1}cm^{-2}$ can be achieved using N_2/H_2 as feedstock and up to 6.95×10^{-9} mol $s^{-1}cm^{-2}$ using N_2/natural gas. In 2009, the novel Solid State Ammonia Synthesis (SSAS) configuration using the Ag-Ru/MgO cathode developed by Skodra and Staukides [106] was able to directly use water as a source of hydrogen. Other than the configurations mentioned above, the oxygen-ion (O^{2-}) conductor has also been shown to be used for ammonia synthesis in SSAS where both processes of electrolysis and ammonia synthesis occur at the cathode but have suffered very low ammonia production rates [106,107].

In intermediate electrocatalysis processes with operating temperatures ranging from 500 °C to 100 °C, molten salts are typically used as electrolytes. Murakami et al. [108] made the earliest study in this temperature range in 2003, using a molten salt mixture electrolyte and porous nickel as electrodes. Other sources of hydrogen, such as water steam [109,110], hydrogen chloride [111], methane [112] and hydrogen sulphide [113], have also been tested. More recently, Licht et al. [114] used a similar configuration for the experiment with NaOH/KOH as electrolyte and nickel as the electrode but added a Fe_2O_3 nanoparticle catalyst to the molten salt. The maximum forming rate of ammonia 1×10^{-8} mols^{-1}cm^{-2} could be achieved by this setup, although it is much lower compared to the works of Murakami's group.

In low-temperature electrochemical ammonia synthesis below 100 °C, Nafion and Sulfonate Polysulfone (SPSF) are commonly used as proton electrolyte conductors [103]. Kordali et al. [115] in 1999 reported a novel configuration that could synthesise ammonia below 100 °C using a combination of the Nafion membrane and KOH solution. The anode was Pt, while the anode was carbon cloth on which Ru had been deposited. The hydrogen source was either hydrogen gas or water. A summary of the selected electrochemical system by previous studies is presented in Table 8.

Table 8. A summary of the selected electrocatalytic ammonia synthesis by previous studies.

Temperature	Electrolyte	Cathode/Anode	NH_3 Yield ($\times 10^{-9}$ mol/s.cm^2)	FE (%)	Ref
High (T > 500 °C)	SCY	Pd	4.50	78	[116]
	BCN	Ag-Pd	1.42	-	[117]
	BCZN	Ag-Pd	1.82	-	[117]
	BCNN	Ag-Pd	2.16	-	[117]
	BCS	Ag-Pd	5.23	-	[118]
	BCGS	Ag-Pd	5.82	-	[118]
	BZCY	Ni- BZCY/Rh	2.86	6.2	[119]
	LSGM	Ag-Pd	2.37	70	[120]
	LCZ	Ag-Pd	2.00	-	[121]
	LCC	Ag-Pd	1.30	-	[121]
	LCZ	Ag-Pd	1.76	80	[122]
	BCG	Ag-Pd	3.09	-	[123]
	BCY1	Ag-Pd	2.10	60	[124]
	BZCY	Ni- BZCY/Cu	1.70	2.7	[125]
	BZCY	Ni- BZCY/Cu	4.10	10	[125]
	BCY2 − ZnO	Ag-Pd	2.60	45	[126]
	CYO − $Ca_3(PO_4)_2/K_3PO_4$	Ag-Pd	9.50	-	[105]
	CYO − $Ca_3(PO_4)_2/K_3PO_4$	Ag-Pd	6.95	-	[104]
	CSO	Ag-Pd	7.20	-	[127]
	CGO	Ag-Pd	7.50	-	[127]
	CYO	Ag-Pd	7.70	-	[127]
	CLO	Ag-Pd	8.20	-	[127]
	LCGM	Ag-Pd	1.63	47	[128]
	LSGM	Ag-Pd	2.53	73	[128]
	LBGM	Ag-Pd	2.04	60	[128]
	LBGM	Ag-Pd	1.89	60	[129]

Table 8. *Cont.*

Temperature	Electrolyte	Cathode/Anode	NH_3 Yield ($\times 10^{-9}$ mol/s.cm^2)	FE (%)	Ref
Intermediate (100 °C < T < 500 °C)	BCG2	Ag-Pd/Ni- BCG	5.00	70	[130]
	BCZS	Ag-Pd	2.67	50	[131]
	BCC	Ag-Pd	2.69	50	[132]
	(Li, Na, K)$_2$CO$_3$-CSO	LSFC/Ni- CSO	5.39	7.5	[133]
	LiCl-KCl-CsCl	Porous Ni Plate	3.33	72	[108]
	LiCl-KCl-CsCl	Al/Porous Ni Plate	33.3	72	[134]
	LiCl-KCl-CsCl	Porous Ni Plate/Baron-doped diamond	5.80	80	[111]
	LiCl-KCl-CsCl	Porous Ni Plate/Glassy carbon rod	20	23	[109]
Low (T < 100 °C)	NaOH/KOH/Nano-Fe_2O_3	Ni	10	35	[114]
	$Na_{0.5}K_{0.5}$OH/Nano-Fe_2O_3	Monel/Ni	16.2	76	[135]
	NaOH-KOH molten salt	(Fe_2O_3/AC)/Ni	8.27	13.7	[136]
	Nafion	SBCF/Ni-CSO	6.90	-	[137]
	Nafion	SBCF/Ni-CSO	7.20	-	[137]
	Nafion	SBCC/Ni-CSO	8.70	-	[137]
	Nafion	Pt	3.13	2.2	[138]
	Nafion	Pt	3.50	0.7	[138]
	Nafion	Pt	1.14	0.55	[138]
	SPSF	SSC/NiO−CSO	6.50	-	[139]
	SPSF	NiO−CSO	2.40	-	[139]
	Nafion	SSN/NiO−CSO	10.5	-	[140]
	SPSF	SSN/NiO−CSO	10.3	-	[141]
	Nafion	SFCN/NiO−CSO	11.3	90.4	[141]
	Nafion	MOF (Fe)/Pt	2.12	1.43	[142]
	Nafion	MOF (Co)/Pt	1.64	1.06	[142]
	Nafion	MOF (Cu)/Pt	1.24	0.96	[142]
	Nafion	MOF (Fe)/Pt	1.52	0.88	[142]
	Nafion	Rh NNs/Carbon rod	6.24	0.7	[143]
	Nafion	Carbon nanospikes/Pt	1.59	11.56	[144]

Note: SCY denotes $ScCe_{0.95}Yb_{0.05}O_{3-\alpha}$, BCN denotes $Ba_3(Ca_{1.18}Nb_{1.82})O_{9-\delta}$, BCZN denotes $Ba_3CaZr_{0.5}Nb_{1.5}O_{9-\delta}$, BCNN denotes $Ba_3Ca_{0.9}Nd_{0.28}Nb_{1.82}O_{9-\delta}$, BCS denotes $BaCe_{0.9}Sm_{0.1}O_{3-\delta}$, BCGS denotes $BaCe_{0.8}Gd_{0.1}Sm_{0.1}O_{3-\delta}$, BZCY denotes $BaZr_{0.7}Ce_{0.2}Y_{0.1}O_{3-\delta}$, LSGM denotes $La_{0.9}Sr_{0.1}Ga_{0.8}Mg_{0.2}O_{3-\alpha}$, LCZ denotes $La_{1.95}Ca_{0.05}Zr_2O_{7-\delta}$, LCC denotes $La_{1.95}Ca_{0.05}Ce_2O_{7-\delta}$, BCG1 denotes $BaCe_{0.8}Gd_{0.2}O_{3-\delta}$, BCY1 denotes $BaCe_{0.85}Y_{0.15}O_{3-\alpha}$, BCY2 denotes $Ba_{0.98}Ce_{0.8}Y_{0.2}O_{3-\alpha}$, CYO denotes $Ce_{0.8}Y_{0.2}O_{1.9}$, CSO denotes $Ce_{0.8}Sm_{0.2}O_{1.9}$, CGO denotes $Ce_{0.8}Gd_{0.2}O_{1.9}$, CLO denotes $Ce_{0.8}La_{0.2}O_{1.9}$, LCGM denotes $La_{0.9}Ca_{0.1}Ga_{0.8}Mg_{0.2}O_{3-\alpha}$, LSGM denotes $La_{0.9}Sr_{0.1}Ga_{0.8}Mg_{0.2}O_{3-\alpha}$, LBGM denotes $La_{0.9}Ba_{0.1}Ga_{0.8}Mg_{0.2}O_{3-\alpha}$, BCG2 denotes $BaCe_{0.85}Gd_{0.15}O_{3-\alpha}$, BCZS denotes $BaCe_{0.7}Zr_{0.2}Sm_{0.1}O_{3-\alpha}$, BCC denotes $BaCe_{0.9}Ca_{0.1}O_{3-\alpha}$, LSFC denotes $La_{0.6}Sr_{0.4}Fe_{0.8}Cu_{0.2}O_{3-\delta}$, SBCF denotes $SmBaCuFeO_{5+\delta}$, SBCC denotes $SmBaCuCoO_{5+\delta}$, SSC denotes $Sm_{0.5}Sr_{0.5}CoO_{3-\delta}$, SSN denotes $Sm_{1.5}Sr_{0.5}NiO_4$, SFCN denotes $SmFe_{0.7}Cu_{0.1}Ni_{0.2}O_3$.

4.3. Plasmacatalysis

The plasmacatalysis process was described as a possible alternative to many chemicals' high-temperature and pressure synthesis systems. In addition to positive and negative ions, plasma often contains a large number of neutral particles, such as atoms, molecules, radicals and excited particles, resulting in highly reactive physical and chemical reactions when used in chemical synthesis. The plasma's ionised and excited species concentration is considerably higher than the traditional thermally heated gas phases. These properties can, therefore, benefit from attaining further effective interaction even without a catalyst [145]. In the interaction of plasma and catalyst, plasma creates a more active spot yielding to higher catalytic activity. When the beneficial effect of plasma and catalyst is combined effectively, it is likely to produce a much higher yield [146].

Depending on the thermal equilibrium or not, plasma could be classified into thermal and non-thermal plasma (NTP). The temperature of plasma, like that of any other gas, is determined by the average energies of the plasma particles (neutral and charged) and their

degrees of freedom (translational, rotational, vibrational and those related to electronic excitation) [147,148]. Plasmas can thus exhibit multiple temperatures as a multi-component system. In common electrical discharge for plasma generation, energy is transferred to heavy articles by collision with electron. In thermal plasma, electron and heavy particles achieved thermal equilibrium due to joule heating. Joule heating or ohmic heating define the process in which the energy of an electric current is converted into heat as it flows through a resistance. The temperature of the gas in thermal plasma is extremely high, typically ranging from 4000 K to 20,000 K. On the other hand, non-thermal plasma is characterised by multiple different temperatures related to different plasma particles and different degrees of freedom. In non-thermal plasma, thermal equilibrium between electron and heavy particles is not achieved, and the temperature of the NTP may be as low as room temperature, although the electron, the excited and the ionised species have a high temperature ($Te >> T_0$) [147].

The temperature of the gas in thermal plasma is extremely high, typically ranging from 4000 K to 20,000 K and is equivalent to that of the electron, which has achieved a thermodynamic equilibrium between the electron and other species. On the other hand, the temperature of the NTP may be as low as room temperature, although the electron, the excited and the ionised species have a high temperature. Since NTP offers less power input, this plasma is a more attractive option for chemical synthesis.

Many researchers have explored the mechanism of plasmacatalytic synthesis of ammonia since the 1900s. The first attempt to utilise plasma to synthesis ammonia can be traced back to 1929 when Brewer et al. [149] successfully synthesised ammonia using glow discharge plasma and achieved an energy yield of 3.03 g-NH_3/kWh. The system used was complex in that high voltage, vacuum and magnetic fields were applied. The magnetic field was reported to have no significant impact on the yield of ammonia. Since these experiments demonstrated the principle of using plasma to produce ammonia, researchers have begun to conduct detailed investigations into the process of plasma-assisted ammonia synthesis using other types of plasma. Table 9 summarises previous research on plasmacatalytic ammonia synthesis.

Table 9. Summary of previous research on plasma-chemical for ammonia synthesis.

Groups	Catalyst	Pressure (Torr)	H_2/N_2	Flow Rate (mL/min)	NH_3 Yield (%)	Energy Yield (g-NH_3/kWh)	Ref
GD	-	3	3	-	-	3.5	[149]
	Pt	50	3	833.3	2	-	[150]
	Pt	50	3	833.3	7.9	-	[151]
	Pt	7	2.5	-	8.1	0.12	[152]
	$MgCl_2$	10	3	-	-	-	[153]
	Ag	5	0.6	78	80.8	-	[154]
RF	-	4.97	4	20	0.27	-	[155]
	Fe	4.97	4	20	0.35	0.01	[156]
	Au	0.26	4	20	0.2	0.1	[157]
	Ga-In	0.26	4	20	0.3	0.3	[158]
	Ni-MOF-74	0.26	4	20	0.23	0.23	[159]
MW	Rh	2.25	0.56	7.5	11.25	0.01	[160]
	-	760	0.11	15,000	3.1	0.04	[161]
	Co/Al_2O_3	760	1.167	120	0.112	0.01	[162]
DBD	Pd	760	3	-	3.13	-	[163]
	MgO	760	0.8	2266.7	0.33	-	[164]
	-	760	3.56	730	1.36	1.83	[165]
	Ru/alumina	760	3	40	4.36	0.37	[166]
	Ru/alumina	760	3	30	4.62	0.40	[167]
	-	760	6	500	0.74	0.69	[168]
	PZT	760	1	11.5	5.9	0.7	[169]
	Alumina	760	3	60	0.67	0.18	[170]
	Cs-Ru/MgO	760	3	4000	2.41	2.3	[171]

Table 9. *Cont.*

Groups	Catalyst	Pressure (Torr)	H_2/N_2	Flow Rate (mL/min)	NH_3 Yield (%)	Energy Yield (g-NH_3/kWh)	Ref
	PZT	760	3	11.5	0.5	0.75	[172]
	Ru-Mg/alumina	760	4	2000	2.55	35.7	[173]
	Cu	760	1	100	3.5	3.3	[174]
	Ru/alumina	760	1.5	-	-	0.64	[175]
	Ni/silica with $BaTiO_3$	760	3	25	12	0.75	[176]
	Ru/alumina	760	3	1000	0.05	1.9	[176]
	Ru/Si-MCM-41	760	1	-	-	1.7	[177]
	Ni/alumina	760	2	100	2	0.89	[178]
	$MgCl_2$	760	1	4000	-	20.5	[179]

Note: GD: glow discharge, RF: radiofrequency, MW: microwave; DBD: dielectric barrier discharge.

Following the initial study, Eremin et al. [151] revealed that ammonia is formed by surface reactions. Afterwards, Venugopalan et al. [152] achieved high productivity of ammonia on Ag coated quartz. Uyama et al. [156,180] found the formation of nitride in addition to hydrazine and ammonia in their study. Nakajima and Sekiguchi [161] found that when plasma is generated by H_2/N_2 gas mixture, the nitrogen gas activation in the plasma has been depressed by hydrogen while hydrogen injection into the afterglow area increased the production of ammonia. In addition to the plasma mentioned above, dielectric barrier discharge was also widely explored. In 2000, researchers [164] tested MgO as a catalyst in combination with DBD. The result shows that the catalyst could increase the ammonia yield by up to 75% more than a plasma-assisted reaction. The group also studied the synthesis of ammonia from methane and nitrogen without any catalyst and achieved an energy yield of as much as 0.69 g-NH_3/kWh [168]. The use of porous materials for ammonia absorption was also studied by Peng et al. [171]. They found that by using a porous material for ammonia absorption, the rate of ammonia synthesis increases due to the lower gas phase of ammonia. The group also examined some metal catalysts as a promoter for improving Ru loaded on magnesium-oxide particles. Caesium (Cs) was reported as the best promoter and capable of achieving energy yield as high as 2.41 g-NH_3/kWh [171]. Akay and Zhang [181] performed research where barium titanate enhanced by Ni/SiO_2 was used as the catalyst. The overall energy yield of 1.9 g-NH_3/kWh was achieved by this configuration. More recently, in a pulsed DBD plasma reactor, Peng et al. [179] used $MgCl_2$ as a catalyst and ammonia absorber. The study discovered that $MgCl_2$ was effective to store generated ammonia for later extraction. The configuration also achieved a very high energy yield with 20.5 g-NH_3/kWh.

More recently, an attempt was made to synthesis NH_3 in the catalyst-free plasma–water interfaces system based on the batch reactor process. Breakthroughs have recently occurred in which plasmas in contact with water surfaces have achieved significant results, putting the interfaces between plasma and water as an NH_3 reaction locus by using a combination of electrochemical and plasma. In these studies, the metal anode was replaced with N_2-plasma gas and successfully produced up to 0.44 mg/hour of NH_3 on 1 mm^2 plasma–liquid interfaces [182].

5. Ammonia as a Renewable Fuel

5.1. Direct Fuel Cell

Fuel cells are currently intensively examined as a breakthrough candidate for carbon-free power generation. The device provides a highly efficient conversion directly from chemical to electricity and has a low environmental footprint. In an early study, ammonia, which has 17% hydrogen by weight, was proposed for use in PEM fuel cells. Though, due to the low operating temperature of the PEM fuel cell, the thermodynamics decomposition of ammonia cannot occur [183]. On top of that, ammonia is lethal to the Nafion membrane

utilised in PEM fuel cells. Thus, external cracking reactors are required to completely convert ammonia into hydrogen, giving an extra energy input and additional costs [184].

Based on electrolyte and reaction, a direct ammonia-fed fuel cell can be divided into three major systems, alkaline fuel cell (AFC), alkaline membrane fuel cell (AMFC) and solid oxide fuel cells (SOFC). The discussion of each configuration is provided below. Ammonia has been reported as a feed for a fuel cell as early as the 1960s based on the alkaline fuel cell developed by Francis Thomas Bacon [185]. The cells use alkaline electrolytes such as potassium hydroxide (KOH) and platinum cathodes. Most recently, Hejze et al. [186] reported the potential of molten hydroxide (NaOH/KOH) as an electrolyte. Unfortunately, the use of KOH and NaOH is not favourable for air-intake fuel cells since it reacts with CO_2 to form K_2CO_3 and Na_2CO_3 and degrades the performance of the alkaline electrolyte.

Recently, alkaline membrane fuel cells (AMFCs) gained attention from the fuel cell society due to the compatibility with CO_2. As reported by Unlu et al. [187], CO_2 introduced in the cathode has a positive effect on improving fuel cell performance. In a recent development, room temperature AMFC has been developed by Lan and Tao [185]. Compared to fuel cells based on acidic polymer electrolytes, low-cost non-precious catalysts, including MnO_2, silver or nickel, may be used for AMFCs [37]. Moreover, Pt/C, PtRu/C and Ru/C were recently investigated AMFCs and can also be used as anodes [188].

Other types of ammonia fuel cells, namely SOFC, are initially developed to prevent NO_X formation [189]. However, the number of scientists who studied SOFC becomes more intense caused by the potencies of the cell to operate at high temperature, thus overcoming the disadvantage suffered by PEMs. At high temperatures, ammonia can be directly decomposed into hydrogen, normally ranging between 500 and 1000 °C, and hence the need for an external cracking reactor is negated. In addition, there was no evidence of ammonia having a bad effect on the ceramic electrolytes used in SOFCs [190]. Nonetheless, because of the fragility of porcelain materials, SOFCs are usually not appropriate for transport use [191].

Research on SOFC fuel cells can be separated into Oxygen Ion-Conducting Electrolytes (SOFC-O) and Hydrogen Ion-Conducting Electrolyte (SOFC-H), which is also known as proton-conducting electrolytes. The schematic of SOFC-O and SOFC-H fuel cells is illustrated in Figure 7.

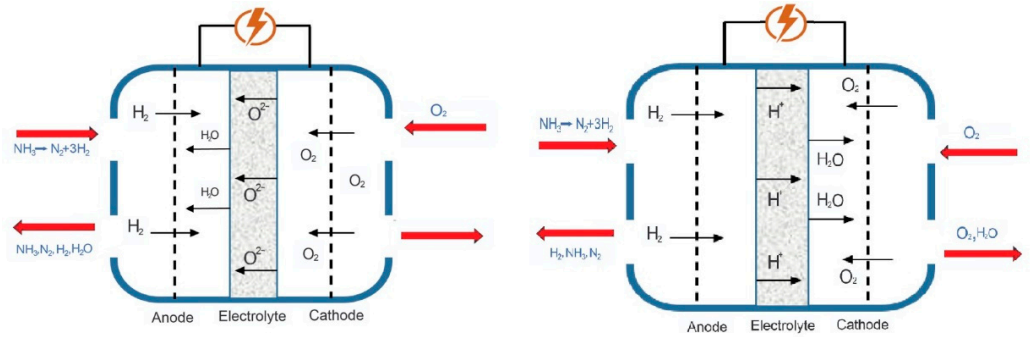

Figure 7. Schematic representation of (**a**) SOFC-O and (**b**) SOFC-H [27].

The SOFC-O operating principle lies in the transportation of oxygen anions across the electrolyte while the charge carrier in SOFC-H is a proton [192]. For both types, ammonia is fed into the anodic site, where it thermally decomposes into nitrogen and hydrogen [193]. In SOFC-O, the oxygen in the cathode compartment is reduced into oxygen ions at the cathode–electrolyte interface and transported across the solid electrolyte, which then reacts with hydrogen electrochemically to produce water [27,194]. The reactions that occur at the anode and cathode are stated below:

$$\text{Anode}: H_2 + O^{2-} \rightarrow H_2O + 2e^- \quad (9)$$

$$\text{Cathode}: \frac{1}{2}O_2 + 2e^- \rightarrow {O_2}^- \quad (10)$$

The SOFC-O electrolytes tend to be built based on solid ceramics with metal oxide. YSZ is most widely used because of its high ionic conversion, which facilitates the efficient movement of oxygen anions through the electrolyte [195]. These solid electrolytes also show strong chemical and thermal stability, which is crucial for the treatment of high temperatures. Samarium doped ceria (SDC)-based electrolytes also sparked interest due to its capability to have high ionic conductivities at lower temperatures [196].

In SOFC-H, the hydrogen in the anode compartment is oxidised into a proton which is then transported across solid electrolyte into the cathode [197]. This later reacts with oxygen to produce water. The reactions that occur at the anode and cathode are given below:

$$\text{Anode}: H_2 \rightarrow 2H^+ + 2e^- \quad (11)$$

$$\text{Cathode}: O_2 + 2H^+ + 2e^- \rightarrow H_2O \quad (12)$$

An SOFC-H system electrolyte is selected based on the conductivity of a proton as well as chemical and mechanical stability. The extraordinarily high proton conductivities of doped $BaCeO_3$(BCO) and $BaZrO_3$(BZO) have been shown over a wide 300 to 1000 °C temperature range [198].

In addition to the qualities of the employed material, electrolyte thickness has a direct effect on fuel cell performance. When a thinner electrolyte has been used, the internal resistance of SOFC decreases. However, reducing electrolyte thickness can affect the mechanical strength and consequently stability over the long term [198]. Table 10 summarises the preceding SOFC fuel cell work that turns ammonia into electricity.

Table 10. Summarization of previous research on SOFC for ammonia synthesis.

Groups	Electrolyte	Thickness (μm)	Cathode	Anode	T(°C)	Power Density (mW/cm^2)	Ref
SOFC-O	YSZ	200	Ag	Pt-YSZ	800–1000	50–125	[199]
	YSZ	400	Ag planar	Ni-YSZ	800	75	[200]
	YSZ	1000	Ag tubular	Ni-YSZ	800	10	[200]
	YSZ	400	Ag	NiO-YSZ	800	60	[196]
	YSZ	150	LSM	NiO-YSZ	700	55	[201]
	YSZ	30	YSZ -LSM	Ni-YSZ	750–850	299	[201]
	YSZ	15	YSZ -LSM	Ni-YSZ	800	526	[202]
	SDC	24	SSC-SDC	NiO-SDC	650	467	[203]
	SDC	10	BSCF	Ni-SDC	700	1190	[204]
SOFC-H	BCGP	1300	Pt	Pt	700	35	[205]
	BCG	1300	Pt	Pt	700	25	[206]
	BCE	1000	Pt	Pt	700	32	[207]
	BCGP	1000	Pt	Ni-BCE	600	23	[208]
	BCG	50	LSC	Ni-BCG	700	355	[209]
	BZCY	35	BSCF	Ni- BZCY	450–700	135–420	[210]
	BCG	30	BSCF	Ni-CGO	600	147	[211]
	BCN	20	LSC	NiO-BCN	700	315	[212]

Note: YSZ denotes yttria-stabilized zirconia, SDC denotes samarium doped ceria, LSM denotes $La_{0.5}Sr_{0.5}MnO_3$, SSC denotes $Sm_{0.5}Sr_{0.5}Co_{3-\delta}$, BSCF denotes $Ba_{0.5}Sr_{0.5}Co_{0.8}Fe_{0.2}O_{3-\delta}$, BCGP denotes $BaCe_{0.8}Gd_{0.19}Pr_{0.01}O_{3-\delta}$, BCG denotes $BaCe_{0.8}Gd_{0.2}O_{3-\delta}$, BCE denotes $BaCe_{0.85}Eu_{0.15}O_3$, LSC denotes $La_{0.5}Sr_{0.5}CoO_{3-\delta}$, BZCY denotes $BaZr_{0.1}Ce_{0.7}Y_{0.2}O_{3-\delta}$, BSCF denotes $Ba_{0.5}Sr_{0.5}Co_{0.8}Fe_{0.2}O_{3-\delta}$, CGO denotes $Ce_{0.8}Gd_{0.2}O_{1.9}$, BCN denotes $BaCe_{0.9}Nd_{0.1}O_{3-\delta}$.

In addition to all of the above forms, microbial fuel cells (MFC) are also seen as an alternate technique for generating electricity directly from ammonia. MFC uses microorganisms in the oxidation process for the conversion of chemical energy from bio-degradable material, for example, ammonia contaminated wastewater. The electrons flow from the anodic side of the external circuit to the cathode, where they combine with the proton and oxygen to form water [198]. The schematic diagram of MFC is shown in Figure 8.

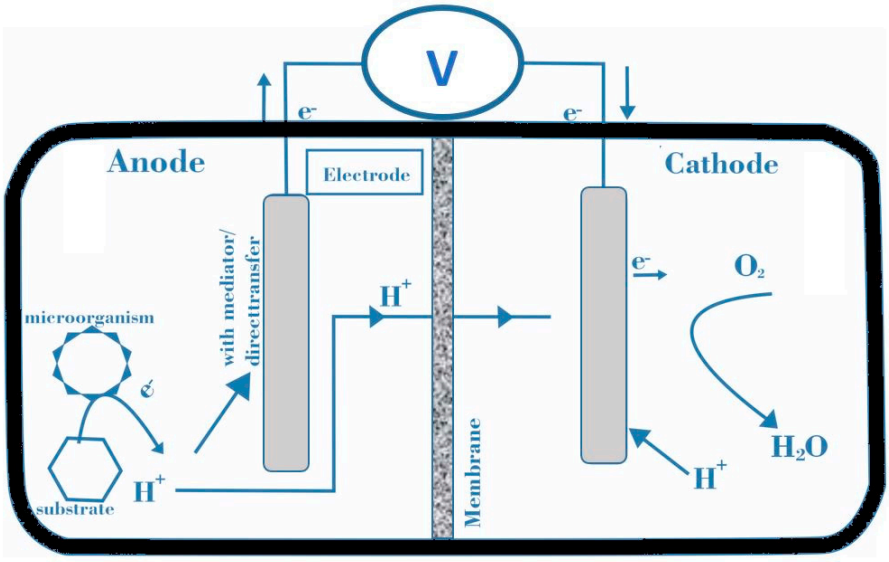

Figure 8. Schematic diagram of MFC [213].

According to Li et al. [214], MFC has been deemed a potential technique for treating wastewater while producing energy, but low power, high cost and reactor scalability issues severely limit its advancement. In addition to wastewater treatment, MFC technology has been proposed as a feasible alternative for air cleaning by removing ammonia from the environment. Yan and Liu [215], in 2020, found Sn-doped V_2O_5 nanoparticles to be a good catalyst for the rapid removal of ammonia in the air using photo-electrocatalysis (PEC) MFCs.

5.2. IC Engine

One of the main industries contributing to GHG emissions worldwide is the transport industry. The search for the right alternative energy source to reduce fossil fuel addiction has been a long, challenging journey. Ammonia-fuelled vehicles, which have received a lot of publicity recently, are one of the solutions to reduce GHG emissions and fossil fuel dependency. Ammonia can be used as fuel in both spark ignition (SI) and compression ignition (CI). Numerous companies and research groups have tested these engines in the last decades. However, ammonia poses undesirable combustion properties, which require further study of its combustion properties. Table 11 compares the characteristics of ammonia with other IC engine fuels.

Table 11. Comparison of NH_3 combustion properties with other fuels at 27 °C [216–220].

	NH_3	H_2	MeOH	DME	Gasoline	Diesel
Storage	L	C	L	L	L	L
Storage pressure (MPa)	1.1	70	0.1	0.5	0.1	0.1
Density (kg m^{-3})	600	39.1	784.6	668	740	820
Laminar burning velocity (m s^{-1})	0.07	3.51	0.36	0.54	0.58	1.28
Low heating value (MJ/kg)	18.8	120	19.92	28.43	42.9	44.41
Latent heat of vaporization (kJ/kg)	1369	0	1100	467	71.78	47.86
Minimum ignition energy (MJ)	8	0.011	0.14	0.29	0.24	0.24
Auto-ignition temperature (K)	930	773–850	712	598–623	530.37	588.7
Octane/cetane number	130	>100	119	55–65	90–98	40–55
AFT (K)	1850	2483	1910	-	2138	-
HCR	1.32	1.41	1.20	-	1.28	-
Explosion limit in air (% vol)	15–28	4.7–75	6.7–36	3.2–18.6	0.6–8	0.6–5.5
Gravimetric hydrogen density (%)	17.8	100	12.5	13	13	12.75

Note: L (liquid); C (compressed); AFT (adiabatic flame temperature); HCR (heat capacity ratio).

Ammonia has low flame velocity, very high auto-ignition temperatures, narrow flammability limits and high vaporisation heat compared to other fuels [217]. Narrow flammability limits and high auto-ignition temperatures create problems for NH_3 to be used in the engine [221]. Although NH_3 can be used as single fuel in the CI engine, extremely higher CR is required to auto-ignite the fuel [222,223]. In addition, high latent heat of vaporisation at the time of injection decreases the gas temperature in the engine, which further complicates it [221]. In the SI engine, the use of ammonia is restricted by low flame velocity and narrow explosion limits resulting in incomplete combustion [224]. Ammonia combustion in the SI-engine can be improved by providing stronger igniters such as plasma jet igniters, smaller combustion chambers to overcome the resistance of NH_3 combustion [223]. Supercharging can also achieve improved combustion [225].

In addition to the problems mentioned above, ammonia also shows low flame speed and specific energy in combination with high ignition energies and high auto-ignition temperatures, resulting in a relatively low propagation rate from the combustion [16]. Although ammonia has been successfully used as mono-fuel both in SI and CI engines, such a low ammonia combustion rate induces inconsistency in combustion under conditions of low engine load or high engine speed [225]. Thereby, it is essential to mix with secondary fuel to overcome its disadvantages as a fuel. In addition to ammonia, potential fuels to be used in SI engines are hydrogen, methanol, ethanol, ethane and gasoline. For CI engines, fuels with higher cetane numbers are preferred as a combustion promoter due to the better ignition characteristics [223]. However, these approaches require some special features [16].

On a dual fuel CI engine, ammonia could be used up to 95% of the fuel energy basis with diesel as a combustion promoter. An optimal mixture, however, is 60% of ammonia on an energy basis because a smaller amount of ammonia would limit the flammability of ammonia [226]. Other studies suggested that an optimal content of ammonia is between 60–80% based on the mass basis [225]. A demonstration of biodiesel as a combustion promoter by Kong et al. [227] revealed that the fuel performed similar engine performance characteristics with ammonia/diesel blends. The operating characteristics are, however, different when Dimethyl Ether (DME) is used as the ammonia fuel combustion promoter. The study shows that ammonia could be used up to 80% only when DME is used as a combustion promoter [217]. Moreover, the study also revealed that the fuel mix of ammonia and DME has a competitive energy cost with current diesel fuel. Even the addition of NH_3 in the blend has been shown to significantly raise emissions of CO, HC and NOx [228].

On the SI engine, gasoline is used as a combustion promoter in most of the studies. A compression ratio of 10:1 is required to get optimal operation of the engine with ammonia content 70% [229]. Gaseous fuels are chosen for SI-engines due to the same phase with ammonia gas, while anhydrous ammonia would lower the temperature of the in-cylinder, thus adversely affecting subsequent turbulence triggering deteriorated combustion and misfire [228]. In the SI engine powered by ammonia/gasoline, gasoline is port-injected while ammonia gas is direct-injected. Direct injection of ammonia gas substantially lowers the cylinder temperature due to the high latent heat of ammonia. Thus, creating turbulence in the combustion chamber will enhance the combustion of the fuel. However, too small swirls do not affect the combustion, while too large swirls have a negative effect on the combustion by blowing out the flames due to the slow propagation of the ammonia flames [223].

Another alternative is by using hydrogen as a secondary fuel by installing an on-board reformer to split ammonia into hydrogen and nitrogen [230]. Morch et al. [219] give a complete database of SI engine performance with ammonia/hydrogen mixture as a fuel. Ammonia and hydrogen have, in this investigation, been incorporated into the CFR engine intake manifold. A series of studies were undertaken with different excess air ratios and hydrogen ammonia ratios. The results revealed that a fuel mixture with 10 vol.% hydrogens has the best performance in terms of efficiency and power. In a comparison study with gasoline, there is a high possibility that an increase in efficiency and power is caused by a greater compression ratio. The analysis of the system has also shown that most of the heat

required can be covered by the exhaust heat. The diagram showing the fuel system setup for the experiments is given in Figure 9.

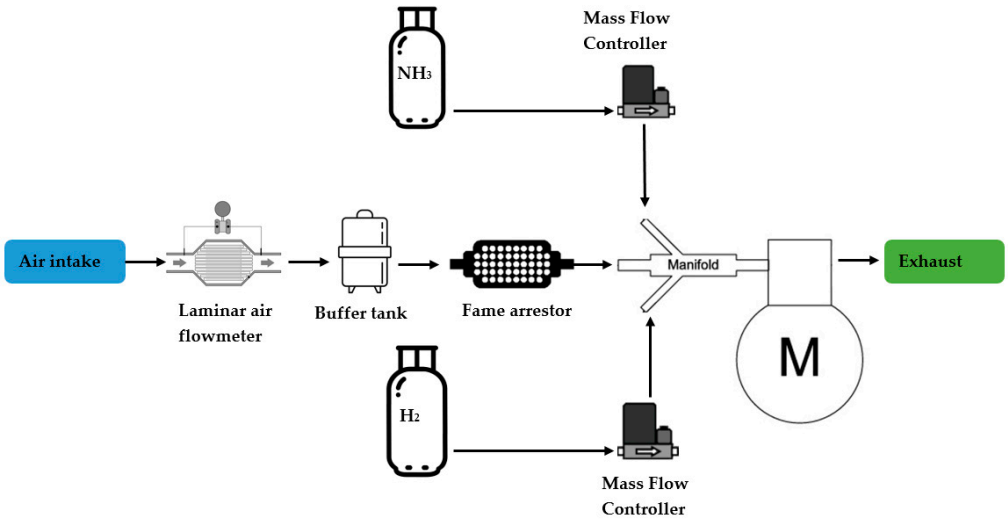

Figure 9. Diagram showing the fuel system setup for the experiments [219].

Much farther trials of ammonia/hydrogen-fuelled engines were also applied to more commercial applications in Italy, where a prototype for electric vehicles with a 15 kW engine was built. The study found that the optimal performance in full load is achieved with 7% of hydrogen content while only 5% in half-load [219]. More recently, Ezzat and Dincer [231] proposed, thermodynamically analysed and compared two different integrated systems of an ammonia/hydrogen-fuelled engine. The first system is made up of hydrogen production. In the second system, an ammonia fuel cell is added to complement the IC engine. The study shows that the first system has higher energy and exergy efficiency with 61.89% and 63.34%, compared to the second system with 34.73% and 38.44%, respectively. The study also shows that when compared with pure ammonia injection, the use of hydrogen from cracked ammonia is extremely beneficial. In addition to road transportations, ammonia is also a favourable fuel for marine industries [232,233]. Unlike the automotive industry, marine systems are not space-constrained, so that catalytic equipment can be deployed for NOx reduction solutions. In the recent development, MAN Energy Solutions replaces the 3000 B&W double-fuel engines operating in the field of LPG and diesel engines [234].

5.3. Gas Turbine

The ammonia-fuelled gas turbine seems destined to become one of the key technologies in the sustainable energy economy of the future. In the 1960s, an early attempt was made to use ammonia as fuel in the gas turbine. However, due to nitrogen molecule in its structure, ammonia combustion is always associated with the formation of nitrogen oxides which exceed current standards [235,236]. Moreover, a longer residence time in the combustion chamber is required for ammonia to be completely combustible due to low laminar burning velocity, which makes it difficult to achieve stable combustion [16]. It also might cause an ammonia slip [237]. Therefore, ammonia-fuelled gas turbines were poorly studied in early development. However, the shift towards carbon-free alternative energy carriers has returned interest in ammonia, including the utilisation in power industries. Burning NH_3 in turbines is the most promising direction of using ammonia as a carrier of surplus electricity generated from renewable energy to balance seasonal energy demand. Thus, many efforts have been devoted to overcoming these shortcomings.

Kobayashi et al. [238] have produced a review article covering the current ammonia combustion research and future directions. The study emphasised that the final product of ammonia combustion is not nitric oxides because the overall reaction is $4NH_3 + 3O_2 \rightarrow 2N_2 + 6H_2O$. This implies that the configuration of the parameters of the combustion

system is crucial to perform the reaction according to this direction. Karabeyoglu et al. [239] developed a test rig and conducted a series of trials with a pre-burner system to partially crack ammonia into H_2. The study revealed that ammonia combustion could be self-sustained when 10% cracking is applied. In 2014, Iki et al. [240] developed a 50 kWe micro gas-turbine system that enables a bi-fuel supply of kerosene and ammonia. The system was able to achieve over 25-kWe power generation by supplying about 10% heat from ammonia gas. In 2015, Iki et al. [241] were able to achieve 21 kWe by replacing the standard combustor with a prototype combustor. The gas turbine performance showed an efficiency of combustion up to 96% with NOx emission above 1000 ppm at 16% O_2. Hayakawa et al. [242] investigated stretching limits for high-pressure flames and observed lower NO formation with higher mixture pressure. Okafor et al. [243], in their experiment and numerical calculations, concluded that predominant rate-limiting reactions in methane–ammonia flames are belonging to the ammonia oxidation path, which controls H and OH radicals. These radicals influence the burning velocity.

$$NO + NH_2 \rightarrow NNH + OH \quad (13)$$

$$NH_2 + O \rightarrow HNO + H \quad (14)$$

$$HNO + H \rightarrow NO + H_2 \quad (15)$$

The study also revealed that the NO concentration decreases when ammonia increases under rich conditions.

In 2016, Ito et al. [244] developed a gas-turbine combustion system with controlled emissions, which uses a mixture of NH_3 and natural gas as the fuel. Combustion properties have been explored via the use of a swirl burner, generally employed in gas turbines, experimentally and numerically. Detailed compositions of the burner exhaust gas were measured under atmospheric pressure and lean fuel circumstances. The results show that with this system, the combustion efficiency above 97% can be achieved for an ammonia mixing ratio below 50%. The study also shows that with an increase of equivalency ratio, unburned species such as NH_3, CO and THC decrease while NO and N_2O emissions increase. The study concludes that low emissions and good combustion efficiency are difficult to obtain in a single-stage reactor.

In 2017, Onishi et al. [245] attempted to create novel ways for reducing NOx emissions while burning an ammonia-natural gas combination in a gas turbine combustor. The concept of low-emission combustion in two-stage combustion was examined numerically and experimentally. In the main zone, methane and ammonia are used as fuel. The secondary zone is then only supplied ammonia. The results indicated two methods for attaining low NOx combustion: rich-lean combustion and a combination of lean combustion and extra ammonia delivery. In the first technique, NOx is created only in the main zone when the fuel is abundant, and the burnt gas is diluted in the secondary zone by secondary air. As a result, primary zone NOx production dominates emission. A lean combustion state in the primary zone results in a low temperature and oxygen concentration in the secondary zone in the second approach. The NOx concentration at the combustor outlet is low as a result of these circumstances. These expected combustion qualities have been experimentally validated. The experimental findings showed that the NOx emission behaviour corresponded to the numerical results.

In 2018, Ito et al. [246] studied a mixture of ammonia and natural gas fuel in a 2 MWe gas turbine. Their results indicated that ammonia is suitable for use in large turbines. Before ammonia is fed to the combustor, the gas turbine power is raised up to 2 MWe using natural gas. The ammonia's heat input ratio to total fuel is used to calculate the ammonia feed to the engine. The result shows that the gas turbine engine's operation was shown to be steady across a wide variety of ammonia mixing ratios ranging from 0% to 20%. As the ratio of ammonia in the mixture increases, the concentration of NOx at the turbine outlet rises significantly up to 5% mixing ratio, then remains steady until it reaches 20%.

6. Conclusions

Ammonia is among the most commonly shipped bulk-produced chemicals, marketed for more than a decade in mass all over the globe. Originally used in the chemical industries and as an intermediate for the production of fertilisers, ammonia has also been explored recently as a hydrogen storage media and a substitute fuel for hydrocarbon. Unlike the conventional ammonia production process that used natural gas as a feedstock and is responsible for carbon emission, ammonia is a means of renewable energy storage formulated from H_2 generated by an electrically driven electrolyser and N_2 separate from the atmospheric air. In addition to that, innovative approaches, such as photocatalysis, electrocatalysis and plasmacatalysis, have attracted widespread interest in ammonia synthesis today. Thus, the application of ammonia as a renewable energy carrier not only plays a key role to lower GHG emissions but also allows transporting H_2 efficiently and economically, permits the direct conversion to electricity by fuel cell and provides versatility in its use, as fuel for the IC engine and power generation. Thus, the ease of processing, transporting and using NH_3 makes it an appealing choice to serve as the link between renewable energy production and demands. However, work is still needed to improve the efficiency of the conversion process for the chemical to compete with hydrocarbon fuel.

Author Contributions: Original draft preparation, M.H.H.; Supervision, T.M.I.M. and M.M.; Review and Editing, H.C.O. and I.M.R.F. Revision, A.S.S.; and F.H. All authors have read and agreed to the published version of the manuscript.

Funding: This research received no external funding.

Acknowledgments: This study was carried out under the International Research Scholarship (IRS) and UTS Presidential Scholarship (UTSP) program, funded by the University of Technology Sydney, Australia.

Conflicts of Interest: The authors declare no conflict of interest.

References

1. Cavicchioli, R.; Ripple, W.J.; Timmis, K.N.; Azam, F.; Bakken, L.R.; Baylis, M.; Behrenfeld, M.J.; Boetius, A.; Boyd, P.W.; Classen, A.T. Scientists' warning to humanity: Microorganisms and climate change. *Nat. Rev. Microbiol.* **2019**, *17*, 569–586. [CrossRef] [PubMed]
2. Edenhofer, O. *Climate Change 2014: Mitigation of Climate Change*; Cambridge University Press: Cambridge, UK, 2015; Volume 3.
3. Lüthi, D.; Le Floch, M.; Bereiter, B.; Blunier, T.; Barnola, J.-M.; Siegenthaler, U.; Raynaud, D.; Jouzel, J.; Fischer, H.; Kawamura, K. High-resolution carbon dioxide concentration record 650,000–800,000 years before present. *Nature* **2008**, *453*, 379–382. [CrossRef] [PubMed]
4. Pachauri, R.K.; Allen, M.R.; Barros, V.R.; Broome, J.; Cramer, W.; Christ, R.; Church, J.A.; Clarke, L.; Dahe, Q.; Dasgupta, P. *Climate Change 2014: Synthesis Report. Contribution of Working Groups I, II and III to the Fifth Assessment Report of the Intergovernmental Panel on Climate Change*; IPCC: Geneva, Switzerland, 2014.
5. United Nations Framework Convention on Climate Change. 1992. Available online: https://unfccc.int/files/essential_background/background_publications_htmlpdf/application/pdf/conveng.pdf (accessed on 13 January 2021).
6. Olivier, G.J.; Peters, J.A. *Trends In Global CO_2 and Total Greenhouse Gas Emissions: 2017 Report*; PBL Netherlands Environmental Assessment Agency: The Hague, The Netherland, 2017.
7. Jiang, X.; Guan, D. The global CO_2 emissions growth after international crisis and the role of international trade. *Energy Policy* **2017**, *109*, 734–746. [CrossRef]
8. Protocol, K. United Nations framework convention on climate change. *Kyoto Protoc.* **1997**, *19*. Available online: https://unfccc.int/kyoto_protocol (accessed on 18 January 2021).
9. International Cooperation on Climate Change; United Nations Framework Convention on Climate Change (UNFCCC). Available online: https://www.dfat.gov.au/international-relations/themes/climate-change/Pages/international-cooperation-on-climate-change (accessed on 19 May 2020).
10. Appl, M. The Haber-Bosch heritage: The ammonia production technology. In Proceedings of the 50th Anniversary of the IFA Technical Conference, Seville, Spain, 25–26 September 1997.
11. Klein, D.; Carazo, M.P.; Doelle, M.; Bulmer, J.; Higham, A. *The Paris Agreement on Climate Change: Analysis and Commentary*; Oxford University Press: Oxford, UK, 2017.
12. Myllyvirta, L. Analysis: Coronavirus Temporarily Reduced China's CO2 Emissions by a Quarter; Carbon Brief. 2020. Available online: https://www.carbonbrief.org/analysis-coronavirus-has-temporarily-reduced-chinas-co2-emissions-by-a-quarter (accessed on 8 January 2021).

13. Zhang, R.; Zhang, Y.; Lin, H.; Feng, X.; Fu, T.-M.; Wang, Y. NOx Emission Reduction and Recovery during COVID-19 in East China. *Atmosphere* **2020**, *11*, 433. [CrossRef]
14. Viswanathan, B. Chapter 9—Hydrogen as an Energy Carrier. In *Energy Sources*; Viswanathan, B., Ed.; Elsevier: Amsterdam, The Netherlands, 2017; pp. 161–183.
15. Edwards, P.; Kuznetsov, V.; David, W. Hydrogen energy. *Philos. Trans. R. Soc. A Math. Phys. Eng. Sci.* **2007**, *365*, 1043–1056. [CrossRef]
16. Valera-Medina, A.; Xiao, H.; Owen-Jones, M.; David, W.I.; Bowen, P.J. Ammonia for power. *Prog. Energy Combust. Sci.* **2018**, *69*, 63–102. [CrossRef]
17. Paris 2015: Tracking Country Climate Pledges. 2017. Available online: https://www.carbonbrief.org/paris-2015-tracking-country-climate-pledges (accessed on 24 June 2020).
18. Innovation Promotion Program Energy Carriers. SIP 2016. Available online: https://www8.cao.go.jp/cstp/panhu/sip_english/20-23.pdf (accessed on 8 January 2021).
19. Crolius, S.H. Ammonia Included in Japan's International Resource Strategy. 2020. Available online: https://www.ammoniaenergy.org/articles/ammonia-included-in-japans-international-resource-strategy/ (accessed on 18 May 2020).
20. Brown, T. Green Ammonia Plants Win Financing in Australia and New Zealand. 2020. Available online: https://www.ammoniaenergy.org/articles/green-ammonia-plants-win-financing-in-australia-and-new-zealand/ (accessed on 19 May 2020).
21. Service, R.F. Ammonia—A Renewable Fuel Made From Sun, Air, and Water—Could Power the Globe Without Carbon. 2018. Available online: https://www.sciencemag.org/news/2018/07/ammonia-renewable-fuel-made-sun-air-and-water-could-power-globe-without-carbon# (accessed on 17 May 2020).
22. Pattabathula, V.; Richardson, J. Introduction to Ammonia Production. 2016. Available online: https://www.aiche.org/resources/publications/cep/2016/september/introduction-ammonia-production (accessed on 15 May 2020).
23. Nitrogen Statistics and Information. 2020. Available online: https://www.usgs.gov/centers/nmic/nitrogen-statistics-and-information (accessed on 20 May 2021).
24. Mineral. Commodity Summaries. 2020. Available online: https://pubs.usgs.gov/periodicals/mcs2020/mcs2020,pdf (accessed on 18 June 2020).
25. Egenhofer, C.; Schrefler, L.; Rizos, V.; Marcu, A.; Genoese, F.; Renda, A.; Wieczorkiewicz, J.; Roth, S.; Infelise, F.; Luchetta, G. The Composition and Drivers of Energy Prices and Costs in Energy-Intensive Industries: The Case of Ceramics, Glass and Chemicals. 2014. Available online: http://aei.pitt.edu/50255/1/CEPS_Energy_Prices_Study_Consolidated_version.pdf (accessed on 14 January 2021).
26. Patil, B.; Wang, Q.; Hessel, V.; Lang, J. Plasma N2-fixation: 1900–2014. *Catal. Today* **2015**, *256*, 49–66. [CrossRef]
27. Afif, A.; Radenahmad, N.; Cheok, Q.; Shams, S.; Kim, J.H.; Azad, A.K. Ammonia-fed fuel cells: A comprehensive review. *Renew. Sustain. Energy Rev.* **2016**, *60*, 822–835. [CrossRef]
28. Davis, B.L.; Dixon, D.A.; Garner, E.B.; Gordon, J.C.; Matus, M.H.; Scott, B.; Stephens, F.H. Efficient regeneration of partially spent ammonia borane fuel. *Angew. Chem. Int. Ed.* **2009**, *48*, 6812–6816. [CrossRef]
29. Leigh, G. Haber-Bosch and Other Industrial Processes. In *Catalysts for Nitrogen Fixation*; Springer: Dordrecht, The Netherlands, 2004; pp. 33–54. [CrossRef]
30. Boerner, L.K. Industrial ammonia production emits more CO_2 than any other chemical-making reaction. *Chem. Eng. News* **2019**, *97*. Available online: https://cen.acs.org/environment/green-chemistry/Industrial-ammonia-production-emits-CO2/97/i24#:~{}:text=It%20belched%20up%20to%20about,reaction%20(see%20page%2023) (accessed on 12 February 2021).
31. Snoeckx, R.; Bogaerts, A. Plasma technology–a novel solution for CO 2 conversion? *Chem. Soc. Rev.* **2017**, *46*, 5805–5863. [CrossRef]
32. MacFarlane, D.R.; Choi, J.; Suryanto, B.H.; Jalili, R.; Chatti, M.; Azofra, L.M.; Simonov, A.N. Liquefied sunshine: Transforming renewables into fertilizers and energy carriers with electromaterials. *Adv. Mater.* **2020**, *32*, 1904804. [CrossRef]
33. Yan, Z.; Ji, M.; Xia, J.; Zhu, H. Recent Advanced Materials for Electrochemical and Photoelectrochemical Synthesis of Ammonia from Dinitrogen: One Step Closer to a Sustainable Energy Future. *Adv. Energy Mater.* **2020**, *10*, 1902020. [CrossRef]
34. Xu, H.; Ithisuphalap, K.; Li, Y.; Mukherjee, S.; Lattimer, J.; Soloveichik, G.; Wu, G. Electrochemical Ammonia Synthesis through N_2 and H_2O under Ambient Conditions: Theory, Practices, and Challenges for Catalysts and Electrolytes. *Nano Energy* **2020**, *69*, 104469. [CrossRef]
35. MacFarlane, D.R.; Cherepanov, P.V.; Choi, J.; Suryanto, B.H.R.; Hodgetts, R.Y.; Bakker, J.M.; Vallana, F.M.F.; Simonov, A.N. A Roadmap to the Ammonia Economy. *Joule* **2020**, *4*, 1186–1205. [CrossRef]
36. Wang, L.; Xia, M.; Wang, H.; Huang, K.; Qian, C.; Maravelias, C.T.; Ozin, G.A. Greening ammonia toward the solar ammonia refinery. *Joule* **2018**, *2*, 1055–1074. [CrossRef]
37. Lan, R.; Irvine, J.T.; Tao, S. Ammonia and related chemicals as potential indirect hydrogen storage materials. *Int. J. Hydrog. Energy* **2012**, *37*, 1482–1494. [CrossRef]
38. Kojima, Y. High Purity Hydrogen Generation from Ammonia. 2017. Available online: https://ep70.eventpilotadmin.com/web/page.php?page=IntHtml&project=ACS17FALL&id=2747276 (accessed on 22 January 2021).
39. Makepeace, J.W.; He, T.; Weidenthaler, C.; Jensen, T.R.; Chang, F.; Vegge, T.; Ngene, P.; Kojima, Y.; de Jongh, P.E.; Chen, P. Reversible ammonia-based and liquid organic hydrogen carriers for high-density hydrogen storage: Recent progress. *Int. J. Hydrog. Energy* **2019**, *44*, 7746–7767. [CrossRef]

40. Bartels, R.J.; Pate, M.B.; Olson, N.K. An economic survey of hydrogen production from conventional and alternative energy sources. *Int. J. Hydrog. Energy* **2010**, *35*, 8371–8384. [CrossRef]
41. Schultz, K.R. *Use of the Modular Helium Reactor for Hydrogen Production*; General Atomics (US): San Diego, CA, USA, 2003. Available online: https://www.osti.gov/biblio/821808-use-modular-helium-reactor-hydrogen-production (accessed on 3 February 2021).
42. Orhan, M.F.; Dincer, I.; Naterer, G.F. Cost analysis of a thermochemical Cu–Cl pilot plant for nuclear-based hydrogen production. *Int. J. Hydrog. Energy* **2008**, *33*, 6006–6020. [CrossRef]
43. Charvin, P.; Stéphane, A.; Florent, L.; Gilles, F. Analysis of solar chemical processes for hydrogen production from water splitting thermochemical cycles. *Energy Convers. Manag.* **2008**, *49*, 1547–1556. [CrossRef]
44. Bartels, J.R. A Feasibility Study of Implementing an Ammonia Economy. Master's Theses, Iowa State University, Iowa, IA, USA, 2008.
45. Andersson, J.; Grönkvist, S. Large-scale storage of hydrogen. *Int. J. Hydrog. Energy* **2019**, *44*, 11901–11919. [CrossRef]
46. Anhydrous Ammonia Transportation Information. 2007. Available online: http://www.mda.state.mn.us/chemicals/spills/ammoniaspills/transportation.htm (accessed on 15 June 2020).
47. Paster, M. Hydrogen Deliver Options and Issues. Available online: http://www1.eere.energy.gov/hydrogenandfuelcells/analysis/pdfs/paster_h2_delivery.pdf (accessed on 15 June 2020).
48. Appl, M. *Ammonia: Principles and Industrial Practice*; Vch Verlagsgesellschaft Mbh: Weinheim, Germany, 1999. Available online: https://trove.nla.gov.au/work/32581098 (accessed on 15 June 2020).
49. Christensen, C.H.; Johannessen, T.; Sørensen, R.Z.; Nørskov, J.K. Towards an ammonia-mediated hydrogen economy? *Catal. Today* **2006**, *111*, 140–144. [CrossRef]
50. Christensen, C.H.; Sørensen, R.Z.; Johannessen, T.; Quaade, U.J.; Honkala, K.; Elmøe, T.D.; Køhler, R.; Nørskov, J.K. Metal ammine complexes for hydrogen storage. *J. Mater. Chem.* **2005**, *15*, 4106–4108. [CrossRef]
51. Haynes, W.M. *CRC Handbook of Chemistry and Physics*; CRC Press: Boca Raton, FL, USA, 2014.
52. Karabeyoglu, A.; Evans, B. Fuel conditioning system for ammonia fired power plants. In Proceedings of the NH3 Congress, Ames, IA, USA, 1 October 2012; Available online: https://www.ammoniaenergy.org/wp-content/uploads/2021/01/evans-brian.pdf (accessed on 23 January 2021).
53. Cole-Parmer Instrument Company. Chemical Compatibility Database, Ammonia, Anhydrous. 2017. Available online: https://www.coleparmer.co.uk/chemical-resistance (accessed on 10 June 2021).
54. Pincha, M.E.; Heizer, B.L.; McHale, M.P. *Material Compatibility Problems for Ammonia Systems*; SAE Technical Paper: Washington, DC, USA, 1988.
55. Graco, Chemical Compatibility Guide. 2013. Available online: https://www.graco.com/content/dam/graco/ipd/literature/misc/chemical-compatibility-guide/Graco_ChemCompGuideEN-B.pdf (accessed on 9 June 2021).
56. CDC. Ammonia. Available online: https://www.cdc.gov/niosh/idlh/7664417 (accessed on 26 May 2020).
57. Ravishankara, A.; Daniel, J.S.; Portmann, R.W. Nitrous oxide (N_2O): The dominant ozone-depleting substance emitted in the 21st century. *Science* **2009**, *326*, 123–125. [CrossRef]
58. Klerke, A.; Christensen, C.H.; Nørskov, J.K.; Vegge, T. Ammonia for hydrogen storage: Challenges and opportunities. *J. Mater. Chem.* **2008**, *18*, 2304–2310. [CrossRef]
59. Organization, W.H. *Ammonia Health and Safety Guide-Health and Safety Guide 37*; International Programme on Chemical Safety: Geneva, Switzerland, 1990.
60. Ryer-Powder, J.E. Health effects of ammonia. *Plant/Oper. Prog.* **1991**, *10*, 228–232. [CrossRef]
61. Smith, C.; Hill, A.K.; Torrente-Murciano, L. Current and future role of Haber-Bosch ammonia in a carbon-free energy landscape. *Energy Environ. Sci.* **2020**, *13*, 331–344. [CrossRef]
62. Wilkinson, I. Green Ammonia. 2017. Available online: Siemens.com (accessed on 23 January 2021).
63. Schmuecker, J. Schmuecker Pinehurst Farm, l.L.C. Available online: http://solarhydrogensystem.com/ (accessed on 16 June 2020).
64. Cholteeva, Y. Sable Chemicals and Tatanga Energy to Construct Solar Energy Plant in Zimbabwe. Available online: https://www.power-technology.com/news/sable-chemicals-and-tatanga-energy-to-construct-solar-energy-plant-in-zimbabwe/ (accessed on 18 June 2020).
65. Solar Ammonia. 2017. Available online: https://www.yara.com/ (accessed on 13 June 2020).
66. Brown, T. Renewable Ammonia Demonstration Plant Announced in South Australia. 2018. Available online: https://ammoniaindustry.com/renewable-ammonia-demonstration-plant-announced-in-south-australia/ (accessed on 14 June 2020).
67. Rusanov, V.D.; Fridman, A.A.; Sholin, G.V. The physics of a chemically active plasma with nonequilibrium vibrational excitation of molecules. *Sov. Phys. Uspekhi* **1981**, *24*, 447. [CrossRef]
68. Chen, X.; Li, N.; Kong, Z.; Ong, W.-J.; Zhao, X. Photocatalytic fixation of nitrogen to ammonia: State-of-the-art advancements and future prospects. *Mater. Horiz.* **2018**, *5*, 9–27. [CrossRef]
69. Schrauzer, G.; Guth, T. Photolysis of water and photoreduction of nitrogen on titanium dioxide. *J. Am. Chem. Soc.* **2002**, *99*, 7189–7193. [CrossRef]
70. Bourgeois, S.; Diakite, D.; Perdereau, M. A study of TiO2 powders as a support for the photochemical synthesis of ammonia. *React. Solids* **1988**, *6*, 95–104. [CrossRef]

71. Hirakawa, H.; Hashimoto, M.; Shiraishi, Y.; Hirai, T. Photocatalytic conversion of nitrogen to ammonia with water on surface oxygen vacancies of titanium dioxide. *J. Am. Chem. Soc.* **2017**, *139*, 10929–10936. [CrossRef] [PubMed]
72. Ranjit, K.T.; Varadarajan, T.K.; Viswanathan, B. Photocatalytic reduction of dinitrogen to ammonia over noble-metal-loaded TiO_2. *J. Photochem. Photobiol. A Chem.* **1996**, *96*, 181–185. [CrossRef]
73. Lashgari, M.; Zeinalkhani, P. Photocatalytic N2 conversion to ammonia using efficient nanostructured solar-energy-materials in aqueous media: A novel hydrogenation strategy and basic understanding of the phenomenon. *Appl. Catal. A Gen.* **2017**, *529*, 91–97. [CrossRef]
74. Sun, S.; An, Q.; Wang, W.; Zhang, L.; Liu, J.; Goddard, W.A., III. Efficient photocatalytic reduction of dinitrogen to ammonia on bismuth monoxide quantum dots. *J. Mater. Chem. A* **2017**, *5*, 201–209. [CrossRef]
75. Hu, S.; Chen, X.; Li, Q.; Zhao, Y.; Mao, W. Effect of sulfur vacancies on the nitrogen photofixation performance of ternary metal sulfide photocatalysts. *Catal. Sci. Technol.* **2016**, *6*, 5884–5890. [CrossRef]
76. Ye, L.; Han, C.; Ma, Z.; Leng, Y.; Li, J.; Ji, X.; Bi, D.; Xie, H.; Huang, Z. Ni_2P loading on $Cd_{0.5}Zn_{0.5}S$ solid solution for exceptional photocatalytic nitrogen fixation under visible light. *Chem. Eng. J.* **2017**, *307*, 311–318. [CrossRef]
77. Wei, P.; Yang, Q.; Guo, L. Bismuth oxyhalide compounds as photocatalysts. *Prog. Chem.* **2009**, *21*, 1734–1741.
78. Dong, G.; Ho, W.; Wang, C. Selective photocatalytic N_2 fixation dependent on gC_3N_4 induced by nitrogen vacancies. *J. Mater. Chem. A* **2015**, *3*, 23435–23441. [CrossRef]
79. Hu, S.; Chen, X.; Li, Q.; Li, F.; Fan, Z.; Wang, H.; Wang, Y.; Zheng, B.; Wu, G. Fe^{3+} doping promoted N_2 photofixation ability of honeycombed graphitic carbon nitride: The experimental and density functional theory simulation analysis. *Appl. Catal. B Environ.* **2017**, *201*, 58–69. [CrossRef]
80. Ileperuma, O.A.; Tennakone, K.; Dissanayake, W.D.D.P. Photocatalytic behaviour of metal doped titanium dioxide: Studies on the photochemical synthesis of ammonia on Mg/TiO_2 catalyst systems. *Appl. Catal.* **1990**, *62*, L1–L5. [CrossRef]
81. Soria, J.; Conesa, J.; Augugliaro, V.; Palmisano, L.; Schiavello, M.; Sclafani, A. Dinitrogen photoreduction to ammonia over titanium dioxide powders doped with ferric ions. *J. Phys. Chem.* **1991**, *95*, 274–282. [CrossRef]
82. Ileperuma, O.A.; Thaminimulla, C.T.K.; Kiridena, W.C.B. Photoreduction of N_2 to NH_3 and H_2O to H_2 on metal doped TiO_2 catalysts (M = Ce, V). *Sol. Eergy Mater. Sol. Cells* **1993**, *28*, 335–343. [CrossRef]
83. Zhao, W.; Zhang, J.; Zhu, X.; Zhang, M.; Tang, J.; Tan, M.; Wang, Y. Enhanced nitrogen photofixation on Fe-doped TiO_2 with highly exposed (1, 0 1) facets in the presence of ethanol as scavenger. *Appl. Catal. B Environ.* **2014**, *144*, 468–477. [CrossRef]
84. Janet, C.; Navaladian, S.; Viswanathan, B.; Varadarajan, T.; Viswanath, R. Heterogeneous wet chemical synthesis of superlattice-type hierarchical ZnO architectures for concurrent H_2 production and N_2 reduction. *J. Phys. Chem. C* **2010**, *114*, 2622–2632. [CrossRef]
85. Khader, M.M.; Lichtin, N.N.; Vurens, G.H.; Salmeron, M.; Somorjai, G.A. Photoassisted catalytic dissociation of water and reduction of nitrogen to ammonia on partially reduced ferric oxide. *Langmuir* **1987**, *3*, 303–304. [CrossRef]
86. Hao, Y.; Dong, X.; Zhai, S.; Ma, H.; Wang, X.; Zhang, X. Hydrogenated bismuth molybdate nanoframe for efficient sunlight-driven nitrogen fixation from air. *Chem.–A Eur. J.* **2016**, *22*, 18722–18728. [CrossRef]
87. Miyama, H.; Fujii, N.; Nagae, Y. Heterogeneous photocatalytic synthesis of ammonia from water and nitrogen. *Chem. Phys. Lett.* **1980**, *74*, 523–524. [CrossRef]
88. Khan, T.M.M.; Bhardwaj, R.C.; Bhardwaj, C. Catalytic Fixation of Nitrogen by the Photocatalytic $CdS/Pt/RuO_2$ Particulate System in the Presence of Aqueous [Ru (Hedta) N_2]⊖ Complex. *Angew. Chem. Int. Ed. Engl.* **1988**, *27*, 923–925. [CrossRef]
89. Sun, S.; Li, X.; Wang, W.; Zhang, L.; Sun, X. Photocatalytic robust solar energy reduction of dinitrogen to ammonia on ultrathin MoS_2. *Appl. Catal. B Environ.* **2017**, *200*, 323–329. [CrossRef]
90. Cao, Y.; Hu, S.; Li, F.; Fan, Z.; Bai, J.; Lu, G.; Wang, Q. Photofixation of atmospheric nitrogen to ammonia with a novel ternary metal sulfide catalyst under visible light. *RSC Adv.* **2016**, *6*, 49862–49867. [CrossRef]
91. Zhang, Q.; Hu, S.; Fan, Z.; Liu, D.; Zhao, Y.; Ma, H.; Li, F. Preparation of gC_3N_4/ZnMoCdS hybrid heterojunction catalyst with outstanding nitrogen photofixation performance under visible light via hydrothermal post-treatment. *Dalton Trans.* **2016**, *45*, 3497–3505. [CrossRef] [PubMed]
92. Hu, S.; Li, Y.; Li, F.; Fan, Z.; Ma, H.; Li, W.; Kang, X. Construction of g-$C_3N_4/Zn_{0.11}Sn_{0.12}Cd_{0.88}S_{1.12}$ hybrid heterojunction catalyst with outstanding nitrogen photofixation performance induced by sulfur vacancies. *ACS Sustain. Chem. Eng.* **2016**, *4*, 2269–2278. [CrossRef]
93. Bai, Y.; Ye, L.; Chen, T.; Wang, L.; Shi, X.; Zhang, X.; Chen, D. Facet-dependent photocatalytic N2 fixation of bismuth-rich Bi5O7I nanosheets. *ACS Appl. Mater. Interfaces* **2016**, *8*, 27661–27668. [CrossRef]
94. Li, H.; Shang, J.; Shi, J.; Zhao, K.; Zhang, L. Facet-dependent solar ammonia synthesis of BiOCl nanosheets via a proton-assisted electron transfer pathway. *Nanoscale* **2016**, *8*, 1986–1993. [CrossRef]
95. Li, H.; Shang, J.; Ai, Z.; Zhang, L. Efficient visible light nitrogen fixation with BiOBr nanosheets of oxygen vacancies on the exposed facets. *J. Am. Chem. Soc.* **2015**, *137*, 6393–6399. [CrossRef]
96. Wang, S.; Hai, X.; Ding, X.; Chang, K.; Xiang, Y.; Meng, X.; Yang, Z.; Chen, H.; Ye, J. Light-Switchable Oxygen Vacancies in Ultrafine Bi5O7Br Nanotubes for Boosting Solar-Driven Nitrogen Fixation in Pure Water. *Adv. Mater.* **2017**, *29*, 1701774. [CrossRef]
97. Wang, Y.; Wei, W.; Li, M.; Hu, S.; Zhang, J.; Feng, R. In situ construction of Z-scheme $gC_3N_4/Mg_{1.1}Al_{0.3}Fe_{0.2}O_{1.7}$ nanorod heterostructures with high N_2 photofixation ability under visible light. *RSC Adv.* **2017**, *7*, 18099–18107. [CrossRef]

98. Hu, S.; Zhang, W.; Bai, J.; Lu, G.; Zhang, L.; Wu, G. Construction of a 2D/2D gC_3N_4/rGO hybrid heterojunction catalyst with outstanding charge separation ability and nitrogen photofixation performance via a surface protonation process. *RSC Adv.* **2016**, *6*, 25695–25702. [CrossRef]
99. Cao, S.; Zhou, N.; Gao, F.; Chen, H.; Jiang, F. All-solid-state Z-scheme 3, 4-dihydroxybenzaldehyde-functionalized Ga_2O_3/graphitic carbon nitride photocatalyst with aromatic rings as electron mediators for visible-light photocatalytic nitrogen fixation. *Appl. Catal. B Environ.* **2017**, *218*, 600–610. [CrossRef]
100. Liang, H.; Zou, H.; Hu, S. Preparation of the W $_{18}$ O_{49}/gC_3N_4 heterojunction catalyst with full-spectrum-driven photocatalytic N 2 photofixation ability from the UV to near infrared region. *New J. Chem.* **2017**, *41*, 8920–8926. [CrossRef]
101. Cong, L.; Yu, Z.; Liu, F.; Huang, W. Electrochemical synthesis of ammonia from N_2 and H_2O using a typical non-noble metal carbon-based catalyst under ambient conditions. *Catal. Sci. Technol.* **2019**, *9*, 1208–1214. [CrossRef]
102. Kyriakou, V.; Garagounis, I.; Vasileiou, E.; Vourros, A.; Stoukides, M. Progress in the electrochemical synthesis of ammonia. *Catal. Today* **2017**, *286*, 2–13. [CrossRef]
103. Garagounis, I.; Vourros, A.; Stoukides, D.; Dasopoulos, D.; Stoukides, M. Electrochemical Synthesis of Ammonia: Recent Efforts and Future Outlook. *Membranes* **2019**, *9*, 112. [CrossRef]
104. Wang, B.H.; de Wang, J.; Liu, R.; Xie, Y.H.; Li, Z.J. Synthesis of ammonia from natural gas at atmospheric pressure with doped ceria–$Ca_3(PO_4)_2$–K_3PO_4 composite electrolyte and its proton conductivity at intermediate temperature. *J. Solid State Electrochem.* **2007**, *11*, 27–31. [CrossRef]
105. Wang, B.; Liu, R.; Wang, J.; Li, Z.; Xie, Y. Doped ceria-Ca-3 (PO4) 2-K3PO4 composite electrolyte: Proton conductivity at intermediate temperature and application in atmospheric pressure ammonia synthesis. *Chin. J. Inorg. Chem.* **2005**, *21*, 1551–1555.
106. Skodra, A.; Stoukides, M. Electrocatalytic synthesis of ammonia from steam and nitrogen at atmospheric pressure. *Solid State Ion.* **2009**, *180*, 1332–1336. [CrossRef]
107. Jeoung, H.; Kim, J.N.; Yoo, C.-Y.; Joo, J.H.; Yu, J.H.; Song, K.C.; Sharma, M.; Yoon, H.C. Electrochemical synthesis of ammonia from water and nitrogen using a Pt/GDC/Pt cell. *Korean Chem. Eng. Res.* **2014**, *52*, 58–62. [CrossRef]
108. Murakami, T.; Nishikiori, T.; Nohira, T.; Ito, Y. Electrolytic synthesis of ammonia in molten salts under atmospheric pressure. *J. Am. Chem. Soc.* **2003**, *125*, 334–335. [CrossRef]
109. Murakami, T.; Nohira, T.; Goto, T.; Ogata, Y.H.; Ito, Y. Electrolytic ammonia synthesis from water and nitrogen gas in molten salt under atmospheric pressure. *Electrochim. Acta* **2005**, *50*, 5423–5426. [CrossRef]
110. Murakami, T.; Nohira, T.; Araki, Y.; Goto, T.; Hagiwara, R.; Ogata, Y.H. Electrolytic Synthesis of Ammonia from Water and Nitrogen under Atmospheric Pressure Using a Boron-Doped Diamond Electrode as a Nonconsumable Anode. *Electrochem. Solid State Lett.* **2007**, *10*, E4. [CrossRef]
111. Murakami, T.; Nishikiori, T.; Nohira, T.; Ito, Y. Electrolytic ammonia synthesis from hydrogen chloride and nitrogen gases with simultaneous recovery of chlorine under atmospheric pressure. *Electrochem. Solid-State Lett.* **2005**, *8*, D19–D21. [CrossRef]
112. Murakami, T.; Nohira, T.; Ogata, Y.H.; Ito, Y. Electrolytic ammonia synthesis in molten salts under atmospheric pressure using methane as a hydrogen source. *Electrochem. Solid-State Lett.* **2005**, *8*, D12–D14. [CrossRef]
113. Murakami, T.; Nohira, T.; Ogata, Y.H.; Ito, Y. Electrochemical synthesis of ammonia and coproduction of metal sulfides from hydrogen sulfide and nitrogen under atmospheric pressure. *J. Electrochem. Soc.* **2005**, *152*, D109–D112. [CrossRef]
114. Licht, S.; Cui, B.; Wang, B.; Li, F.-F.; Lau, J.; Liu, S. Ammonia synthesis by N_2 and steam electrolysis in molten hydroxide suspensions of nanoscale Fe_2O_3. *Science* **2014**, *345*, 637–640. [CrossRef]
115. Kordali, V.; Kyriacou, G.; Lambrou, C. Electrochemical synthesis of ammonia at atmospheric pressure and low temperature in a solid polymer electrolyte cell. *Chem. Commun.* **2000**, *17*, 1673–1674. [CrossRef]
116. Marnellos, G.; Stoukides, M. Ammonia synthesis at atmospheric pressure. *Science* **1998**, *282*, 98–100. [CrossRef]
117. Li, Z.; Liu, R.; Xie, Y.; Feng, S.; Wang, J. A novel method for preparation of doped $Ba_3(Ca_{1.18}Nb_{1.82})O_{9-\delta}$: Application to ammonia synthesis at atmospheric pressure. *Solid State Ion.* **2005**, *176*, 1063–1066. [CrossRef]
118. Li, Z.; Liu, R.; Wang, J.; Xu, Z.; Xie, Y.; Wang, B. Preparation of double-doped $BaCeO_3$ and its application in the synthesis of ammonia at atmospheric pressure. *Sci. Technol. Adv. Mater.* **2007**, *8*, 566. [CrossRef]
119. Vasileiou, E.; Kyriakou, V.; Garagounis, I.; Vourros, A.; Stoukides, M. Ammonia synthesis at atmospheric pressure in a $BaCe_{0.2}Zr_{0.7}Y_{0.1}O_{2.9}$ solid electrolyte cell. *Solid State Ion.* **2015**, *275*, 110–116. [CrossRef]
120. Zhang, F.; Yang, Q.; Pan, B.; Xu, R.; Wang, H.; Ma, G. Proton conduction in $La_{0.9}Sr_{0.1}Ga_{0.8}Mg_{0.2}O_{3-\alpha}$ ceramic prepared via microemulsion method and its application in ammonia synthesis at atmospheric pressure. *Mater. Lett.* **2007**, *61*, 4144–4148. [CrossRef]
121. Wang, J.-D.; Xie, Y.-H.; Zhang, Z.-F.; Liu, R.-Q.; Li, Z.-J. Protonic conduction in Ca_{2+}-doped $La_2M_2O_7$ (M= Ce, Zr) with its application to ammonia synthesis electrochemically. *Mater. Res. Bull.* **2005**, *40*, 1294–1302. [CrossRef]
122. Xie, Y.-H.; Wang, J.-D.; Liu, R.-Q.; Su, X.-T.; Sun, Z.-P.; Li, Z.-J. Preparation of $La_{1.9}Ca_{0.}Zr_2O_{6.95}$ with pyrochlore structure and its application in synthesis of ammonia at atmospheric pressure. *Solid State Ion.* **2004**, *168*, 117–121. [CrossRef]
123. Li, Z.-J.; Liu, R.-Q.; Wang, J.-D.; Xie, Y.-H.; Yue, F. Preparation of $BaCe_{0.8}Gd_{0.2}O_{3-\delta}$ by the citrate method and its application in the synthesis of ammonia at atmospheric pressure. *J. Solid State Electrochem.* **2005**, *9*, 201–204. [CrossRef]
124. Guo, Y.; Liu, B.; Yang, Q.; Chen, C.; Wang, W.; Ma, G. Preparation via microemulsion method and proton conduction at intermediate-temperature of $BaCe_{1-x}YxO_{3-\alpha}$. *Electrochem. Commun.* **2009**, *11*, 153–156. [CrossRef]

125. Vasileiou, E.; Kyriakou, V.; Garagounis, I.; Vourros, A.; Manerbino, A.; Coors, W.; Stoukides, M. Electrochemical enhancement of ammonia synthesis in a $BaZr_{0.7}Ce_{0.2}Y_{0.1}O_{2.9}$ solid electrolyte cell. *Solid State Ion.* **2016**, *288*, 357–362. [CrossRef]
126. Zhang, M.; Xu, J.; Ma, G. Proton conduction in $Ba_xCe_{0.8}Y_{0.2}O_{3-\alpha}$ + 0.04ZnO at intermediate temperatures and its application in ammonia synthesis at atmospheric pressure. *J. Mater. Sci.* **2011**, *46*, 4690–4694. [CrossRef]
127. Liu, R.-Q.; Xie, Y.-H.; Wang, J.-D.; Li, Z.-J.; Wang, B.-H. Synthesis of ammonia at atmospheric pressure with $Ce_{0.8}M_{0.2}O_{2-\delta}$ (M= La, Y, Gd, Sm) and their proton conduction at intermediate temperature. *Solid State Ion.* **2006**, *177*, 73–76. [CrossRef]
128. Chen, C.; Wang, W.; Ma, G. Proton conduction in $La_{0.9}M_{0.1c}Ga_{0.8}Mg_{0.2}O_{3-\alpha}$ at intermediate temperature and its application to synthesis of ammonia at atmospheric pressure. *Acta Chim. Sin.* **2009**, *67*, 623–628.
129. Chen, C.; Ma, G. Preparation, proton conduction, and application in ammonia synthesis at atmospheric pressure of $La_{0.9}Ba_{0.1}Ga_{1-x}Mg_xO_{3-\alpha}$. *J. Mater. Sci.* **2008**, *43*, 5109–5114. [CrossRef]
130. Chen, C.; Ma, G. Proton conduction in $BaCe_{1-x}Gd_xO_{3-\alpha}$ at intermediate temperature and its application to synthesis of ammonia at atmospheric pressure. *J. Alloy. Compd.* **2009**, *485*, 69–72. [CrossRef]
131. Wang, X.; Yin, J.; Xu, J.; Wang, H.; Ma, G. Chemical stability, ionic conductivity of $BaCe_{0.9-x}Zr_xSm_{0.10}O_{3-\alpha}$ and its application to ammonia synthesis at atmospheric pressure. *Chin. J. Chem.* **2011**, *29*, 1114–1118. [CrossRef]
132. Liu, J.; Li, Y.; Wang, W.; Wang, H.; Zhang, F.; Ma, G. Proton conduction at intermediate temperature and its application in ammonia synthesis at atmospheric pressure of $BaCe_{1-x}Ca_xO_{3-\alpha}$. *J. Mater. Sci.* **2010**, *45*, 5860–5864. [CrossRef]
133. Amar, I.A.; Petit, C.T.; Zhang, L.; Lan, R.; Skabara, P.J.; Tao, S. Electrochemical synthesis of ammonia based on doped-ceria-carbonate composite electrolyte and perovskite cathode. *Solid State Ion.* **2011**, *201*, 94–100. [CrossRef]
134. Murakami, T.; Nishikiori, T.; Nohira, T.; Ito, Y. Investigation of anodic reaction of electrolytic ammonia synthesis in molten salts under atmospheric pressure. *J. Electrochem. Soc.* **2005**, *152*, D75–D78. [CrossRef]
135. Li, F.-F.; Licht, S. Advances in understanding the mechanism and improved stability of the synthesis of ammonia from air and water in hydroxide suspensions of nanoscale Fe_2O_3. *Inorg. Chem.* **2014**, *53*, 10042–10044. [CrossRef]
136. Cui, B.; Zhang, J.; Liu, S.; Liu, X.; Xiang, W.; Liu, L.; Xin, H.; Lefler, M.J.; Licht, S. Electrochemical synthesis of ammonia directly from N_2 and water over iron-based catalysts supported on activated carbon. *Green Chem.* **2017**, *19*, 298–304. [CrossRef]
137. Zhang, Z.; Zhong, Z.; Ruiquan, L. Cathode catalysis performance of $SmBaCuMO_{5+\delta}$ (M= Fe, Co, Ni) in ammonia synthesis. *J. Rare Earths* **2010**, *28*, 556–559. [CrossRef]
138. Lan, R.; Irvine, J.T.; Tao, S. Synthesis of ammonia directly from air and water at ambient temperature and pressure. *Sci. Rep.* **2013**, *3*, 1–7. [CrossRef]
139. Wang, J.; Liu, R.-Q. Property research of SDC and SSC in ammonia synthesis at atmospheric pressure and low temperature. *Acta Chim. Sin* **2008**, *66*, 717–721.
140. Liu, R.; Xu, G. Comparison of electrochemical synthesis of ammonia by using sulfonated polysulfone and nafion membrane with $Sm_{1.5}$ $Sr_{0.5}$ NiO_4. *Chin. J. Chem.* **2010**, *28*, 139–142. [CrossRef]
141. Xu, G.; Liu, R.; Wang, J. Electrochemical synthesis of ammonia using a cell with a Nafion membrane and $SmFe_{0.7}Cu_{0.3-x}Ni_xO_3$ (x= 0−0.3) cathode at atmospheric pressure and lower temperature. *Sci. China Ser. B Chem.* **2009**, *52*, 1171–1175. [CrossRef]
142. Zhao, X.; Yin, F.; Liu, N.; Li, G.; Fan, T.; Chen, B. Highly efficient metal–organic-framework catalysts for electrochemical synthesis of ammonia from N 2 (air) and water at low temperature and ambient pressure. *J. Mater. Sci.* **2017**, *52*, 10175–10185. [CrossRef]
143. Liu, H.-M.; Han, S.-H.; Zhao, Y.; Zhu, Y.-Y.; Tian, X.-L.; Zeng, J.-H.; Jiang, J.-X.; Xia, B.Y.; Chen, Y. Surfactant-free atomically ultrathin rhodium nanosheet nanoassemblies for efficient nitrogen electroreduction. *J. Mater. Chem. A* **2018**, *6*, 3211–3217. [CrossRef]
144. Song, Y.; Johnson, D.; Peng, R.; Hensley, D.K.; Bonnesen, P.V.; Liang, L.; Huang, J.; Yang, F.; Zhang, F.; Qiao, R. A physical catalyst for the electrolysis of nitrogen to ammonia. *Sci. Adv.* **2018**, *4*, e1700336. [CrossRef] [PubMed]
145. Carreon, M.L. Plasma catalytic ammonia synthesis: State of the art and future directions. *J. Phys. D Appl. Phys.* **2019**, *52*, 483001. [CrossRef]
146. Chen, G.; Wang, L.; Godfroid, T.; Snyders, R. *Progress in Plasma-Assisted Catalysis for Carbon Dioxide Reduction, In Plasma Chemistry and Gas Conversion*; IntechOpen: London, UK, 2018.
147. Fridman, A. *Plasma Chemistry*; Cambridge University Press: Cambridge, UK, 2008.
148. Bruggeman, P.; Sadeghi, N.; Schram, D.; Linss, V. Gas temperature determination from rotational lines in non-equilibrium plasmas: A review. *Plasma Sources Sci. Technol.* **2014**, *23*, 023001. [CrossRef]
149. Brewer, K.A.; Westhaver, J.W. The Synthesis of Ammonia in the Glow Discharge. *J. Phys. Chem.* **1928**, *33*, 883–895. [CrossRef]
150. Maltsev, A.; Churina, L.; Eremin, E. Activity of heterogeneous catalysts in synthesis of ammonia in glow discharge. *Russ. J. Phys. Chem. USSR* **1968**, *42*, 1235.
151. Eremin, E.N.; Maltsev, A.N.; Belova, V.M. Behaviour of a Catalyst in a Glow-discharge Plasma. *Russ. J. Phys. Chem.* **1969**, *43*, 443.
152. Yin, S.K.; Venugopalan, M. Plasma chemical synthesis. *I. Effect of electrode material on the synthesis of ammonia. Plasma Chem. Plasma Process.* **1983**, *3*, 343–350. [CrossRef]
153. Sugiyama, K.; Akazawa, K.; Oshima, M.; Miura, H.; Matsuda, T.; Nomura, O. Ammonia synthesis by means of plasma over MgO catalyst. *Plasma Chem. Plasma Process.* **1986**, *6*, 179–193. [CrossRef]
154. Touvelle, M.; Licea, J.M.; Venugopalan, M. Plasma chemical synthesis. *II. Effect of wall surface on the synthesis of ammonia. Plasma Chem. Plasma Process.* **1987**, *7*, 101–108. [CrossRef]

155. Uyama, H.; Uchikura, T.; Niijima, H.; Matsumoto, O. Synthesis of ammonia with RF discharge. Adsorption of products on zeolite. *Chem. Lett.* **1987**, *16*, 555–558. [CrossRef]
156. Uyama, H.; Matsumoto, O. Synthesis of ammonia in high-frequency discharges. *Plasma Chem. Plasma Process.* **1989**, *9*, 13–24. [CrossRef]
157. Shah, J.; Wang, W.; Bogaerts, A.; Carreon, M.L. Ammonia synthesis by radio frequency plasma catalysis: Revealing the underlying mechanisms. *ACS Appl. Energy Mater.* **2018**, *1*, 4824–4839. [CrossRef]
158. Shah, R.J.; Harrison, J.M.; Carreon, M.L. Ammonia plasma-catalytic synthesis using low melting point alloys. *Catalysts* **2018**, *8*, 437. [CrossRef]
159. Shah, J.; Wu, T.; Lucero, J.; Carreon, M.A.; Carreon, M.L. Nonthermal Plasma Synthesis of Ammonia over Ni-MOF-74. *ACS Sustain. Chem. Eng.* **2018**, *7*, 377–383. [CrossRef]
160. Siemsen, L.G. The Synthesis of Ammonia from Hydrogen and Atomic Nitrogen on the Rh Surfac. 1990. Available online: https://lib.dr.iastate.edu/cgi/viewcontent.cgi?article=12220&context=rtd (accessed on 9 January 2021).
161. Nakajima, J.; Sekiguchi, H. Synthesis of ammonia using microwave discharge at atmospheric pressure. *Thin Solid Film.* **2008**, *516*, 4446–4451. [CrossRef]
162. Bai, X.; Tiwari, S.; Robinson, B.; Killmer, C.; Li, L.; Hu, J. Microwave catalytic synthesis of ammonia from methane and nitrogen. *Catal. Sci. Technol.* **2018**, *8*, 6302–6305. [CrossRef]
163. Eremin, E.; Maltsev, A.; Syaduk, V. Catalytic synthesis of ammonia in a barrier discharge. *Russ. J. Phys. Chem. USSR* **1971**, *45*, 635.
164. Mingdong, B.; Xiyao, B.; Zhitao, Z.; Mindi, B. Synthesis of ammonia in a strong electric field discharge at ambient pressure. *Plasma Chem. Plasma Process.* **2000**, *20*, 511–520. [CrossRef]
165. Bai, M.; Zhang, Z.; Bai, X.; Bai, M.; Ning, W. Plasma synthesis of ammonia with a microgap dielectric barrier discharge at ambient pressure. *IEEE Trans. Plasma Sci.* **2003**, *31*, 1285–1291.
166. Mizushima, T.; Matsumoto, K.; Sugoh, J.-I.; Ohkita, H.; Kakuta, N. Tubular membrane-like catalyst for reactor with dielectric-barrier-discharge plasma and its performance in ammonia synthesis. *Appl. Catal. A Gen.* **2004**, *265*, 53–59. [CrossRef]
167. Mizushima, T.; Matsumoto, K.; Ohkita, H.; Kakuta, N. Catalytic effects of metal-loaded membrane-like alumina tubes on ammonia synthesis in atmospheric pressure plasma by dielectric barrier discharge. *Plasma Chem. Plasma Process.* **2007**, *27*, 1–11. [CrossRef]
168. Bai, M.; Zhang, Z.; Bai, M.; Bai, X.; Gao, H. Synthesis of ammonia using CH_4/N_2 plasmas based on micro-gap discharge under environmentally friendly condition. *Plasma Chem. Plasma Process.* **2008**, *28*, 405–414. [CrossRef]
169. Bai, M.; Zhang, Z.; Bai, M.; Bai, X.; Gao, H. Conversion of methane to liquid products, hydrogen, and ammonia with environmentally friendly condition-based microgap discharge. *J. Air Waste Manag. Assoc.* **2008**, *58*, 1616–1621. [CrossRef]
170. Hong, J.; Aramesh, M.; Shimoni, O.; Seo, D.H.; Yick, S.; Greig, A.; Charles, C.; Prawer, S.; Murphy, A.B. Plasma catalytic synthesis of ammonia using functionalized-carbon coatings in an atmospheric-pressure non-equilibrium discharge. *Plasma Chem. Plasma Process.* **2016**, *36*, 917–940. [CrossRef]
171. Peng, P.; Li, Y.; Cheng, Y.; Deng, S.; Chen, P.; Ruan, R. Atmospheric pressure ammonia synthesis using non-thermal plasma assisted catalysis. *Plasma Chem. Plasma Process.* **2016**, *36*, 1201–1210. [CrossRef]
172. Gómez-Ramírez, A.; Montoro-Damas, A.M.; Cotrino, J.; Lambert, R.M.; González-Elipe, A.R. About the enhancement of chemical yield during the atmospheric plasma synthesis of ammonia in a ferroelectric packed bed reactor. *Plasma Process. Polym.* **2017**, *14*, 1600081. [CrossRef]
173. Kim, H.H.; Teramoto, Y.; Ogata, A.; Takagi, H.; Nanba, T. Atmospheric-pressure nonthermal plasma synthesis of ammonia over ruthenium catalysts. *Plasma Process. Polym.* **2017**, *14*, 1600157. [CrossRef]
174. Aihara, K.; Akiyama, M.; Deguchi, T.; Tanaka, M.; Hagiwara, R.; Iwamoto, M. Remarkable catalysis of a wool-like copper electrode for NH 3 synthesis from N 2 and H 2 in non-thermal atmospheric plasma. *Chem. Commun.* **2016**, *52*, 13560–13563. [CrossRef]
175. Xie, D.; Sun, Y.; Zhu, T.; Fan, X.; Hong, X.; Yang, W. Ammonia synthesis and by-product formation from H_2O, H_2 and N_2 by dielectric barrier discharge combined with an Ru/Al_2O_3 catalyst. *RSC Adv.* **2016**, *6*, 105338–105346. [CrossRef]
176. Patil, B. *Plasma (Catalyst)-Assisted Nitrogen Fixation: Reactor Development for Nitric Oxide and Ammonia Production*; Micro Flow Chemistry and Synthetic Methodology: Eindhoven, The Netherlands, 2017.
177. Peng, P.; Cheng, Y.; Hatzenbeller, R.; Addy, M.; Zhou, N.; Schiappacasse, C.; Chen, D.; Zhang, Y.; Anderson, E.; Liu, Y. Ru-based multifunctional mesoporous catalyst for low-pressure and non-thermal plasma synthesis of ammonia. *Int. J. Hydrog. Energy* **2017**, *42*, 19056–19066. [CrossRef]
178. Mehta, P.; Barboun, P.; Herrera, F.A.; Kim, J.; Rumbach, P.; Go, D.B.; Hicks, J.C.; Schneider, W.F. Overcoming ammonia synthesis scaling relations with plasma-enabled catalysis. *Nat. Catal.* **2018**, *1*, 269–275. [CrossRef]
179. Peng, P.; Chen, P.; Addy, M.; Cheng, Y.; Anderson, E.; Zhou, N.; Schiappacasse, C.; Zhang, Y.; Chen, D.; Hatzenbeller, R. Atmospheric plasma-assisted ammonia synthesis enhanced via synergistic catalytic absorption. *ACS Sustain. Chem. Eng.* **2018**, *7*, 100–104. [CrossRef]
180. Uyama, H.; Nakamura, T.; Tanaka, S.; Matsumoto, O. Catalytic effect of iron wires on the syntheses of ammonia and hydrazine in a radio-frequency discharge. *Plasma Chem. Plasma Process.* **1993**, *13*, 117–131. [CrossRef]
181. Akay, G.; Zhang, K. Process intensification in ammonia synthesis using novel coassembled supported microporous catalysts promoted by nonthermal plasma. *Ind. Eng. Chem. Res.* **2017**, *56*, 457–468. [CrossRef]

182. Hawtof, R.; Ghosh, S.; Guarr, E.; Xu, C.; Sankaran, R.M.; Renner, J.N. Catalyst-free, highly selective synthesis of ammonia from nitrogen and water by a plasma electrolytic system. *Sci. Adv.* **2019**, *5*, eaat5778. [CrossRef]
183. Cheddie, D. *Ammonia as a Hydrogen Source for Fuel Cells: A Review*; InTechOpen: London, UK, 2012.
184. Yu, X.; Ye, S. Recent advances in activity and durability enhancement of Pt/C catalytic cathode in PEMFC: Part, I. Physico-chemical and electronic interaction between Pt and carbon support, and activity enhancement of Pt/C catalyst. *J. Power Sources* **2007**, *172*, 133–144. [CrossRef]
185. Lan, R.; Tao, S. Direct ammonia alkaline anion-exchange membrane fuel cells. *Electrochem. Solid-State Lett.* **2010**, *13*, B83–B86. [CrossRef]
186. Hejze, T.; Besenhard, J.; Kordesch, K.; Cifrain, M.; Aronsson, R. Current status of combined systems using alkaline fuel cells and ammonia as a hydrogen carrier. *J. Power Sources* **2008**, *176*, 490–493. [CrossRef]
187. Unlu, M.; Zhou, J.; Kohl, P.A. Anion exchange membrane fuel cells: Experimental comparison of hydroxide and carbonate conductive ions. *Electrochem. Solid-State Lett.* **2009**, *12*, B27–B30. [CrossRef]
188. Suzuki, S.; Muroyama, H.; Matsui, T.; Eguchi, K. Fundamental studies on direct ammonia fuel cell employing anion exchange membrane. *J. Power Sources* **2012**, *208*, 257–262. [CrossRef]
189. Carrette, L.; Friedrich, K.A.; Stimming, U. Fuel cells: Principles, types, fuels, and applications. *ChemPhysChem* **2000**, *1*, 162–193. [CrossRef]
190. Meng, G.; Ma, G.; Ma, Q.; Peng, R.; Liu, X. Ceramic membrane fuel cells based on solid proton electrolytes. *Solid State Ion.* **2007**, *178*, 697–703. [CrossRef]
191. Li, T.; Rabuni, M.; Kleiminger, L.; Wang, B.; Kelsall, G.; Hartley, U.; Li, K. A highly-robust solid oxide fuel cell (SOFC): Simultaneous greenhouse gas treatment and clean energy generation. *Energy Environ. Sci.* **2016**, *9*, 3682–3686. [CrossRef]
192. Siddiqui, O.; Dincer, I. A review and comparative assessment of direct ammonia fuel cells. *Therm. Sci. Eng. Prog.* **2018**, *5*, 568–578. [CrossRef]
193. Lan, R.; Tao, S. Ammonia as a suitable fuel for fuel cells. *Front. Energy Res.* **2014**, *2*, 35. [CrossRef]
194. Ishak, F.; Dincer, I.; Zamfirescu, C. Thermodynamic analysis of ammonia-fed solid oxide fuel cells. *J. Power Sources* **2012**, *202*, 157–165. [CrossRef]
195. Vayenas, C.; Farr, R. Cogeneration of electric energy and nitric oxide. *Science* **1980**, *208*, 593–594. [CrossRef]
196. Fournier, G.; Cumming, I.; Hellgardt, K. High performance direct ammonia solid oxide fuel cell. *J. Power Sources* **2006**, *162*, 198–206. [CrossRef]
197. Hossain, S.; Abdalla, A.M.; Jamain, S.N.B.; Zaini, J.H.; Azad, A.K. A review on proton conducting electrolytes for clean energy and intermediate temperature-solid oxide fuel cells. *Renew. Sustain. Energy Rev.* **2017**, *79*, 750–764. [CrossRef]
198. Jeerh, G.; Zhang, G.M.; Tao, S. Recent progress in ammonia fuel cells and their potential applications. *J. Mater. Chem. A* **2021**.
199. Wojcik, A.; Middleton, H.; Damopoulos, I. Ammonia as a fuel in solid oxide fuel cells. *J. Power Sources* **2003**, *118*, 342–348. [CrossRef]
200. Choudhary, V.T.; Goodman, D. CO-free fuel processing for fuel cell applications. *Catal. Today* **2002**, *77*, 65–78. [CrossRef]
201. Ma, Q.; Ma, J.; Zhou, S.; Yan, R.; Gao, J.; Meng, G. A high-performance ammonia-fueled SOFC based on a YSZ thin-film electrolyte. *J. Power Sources* **2007**, *164*, 86–89. [CrossRef]
202. Zhang, L.; You, C.; Weishen, Y.; Liwu, L. A direct ammonia tubular solid oxide fuel cell. *Chin. J. Catal.* **2007**, *28*, 749–751. [CrossRef]
203. Liu, M.; Peng, R.; Dong, D.; Gao, J.; Liu, X.; Meng, G. Direct liquid methanol-fueled solid oxide fuel cell. *J. Power Sources* **2008**, *185*, 188–192. [CrossRef]
204. Meng, G.; Jiang, C.; Ma, J.; Ma, Q.; Liu, X. Comparative study on the performance of a SDC-based SOFC fueled by ammonia and hydrogen. *J. Power Sources* **2007**, *173*, 189–193. [CrossRef]
205. Pelletier, L.; McFarlan, A.; Maffei, N. Ammonia fuel cell using doped barium cerate proton conducting solid electrolytes. *J. Power Sources* **2005**, *145*, 262–265. [CrossRef]
206. Maffei, N.; Pelletier, L.; Charland, J.; McFarlan, A. An intermediate temperature direct ammonia fuel cell using a proton conducting electrolyte. *J. Power Sources* **2005**, *140*, 264–267. [CrossRef]
207. Maffei, N.; Pelletier, L.; Charland, J.; McFarlan, A. An ammonia fuel cell using a mixed ionic and electronic conducting electrolyte. *J. Power Sources* **2006**, *162*, 165–167. [CrossRef]
208. Maffei, N.; Pelletier, L.; McFarlan, A. A high performance direct ammonia fuel cell using a mixed ionic and electronic conducting anode. *J. Power Sources* **2008**, *175*, 221–225. [CrossRef]
209. Ma, Q.; Peng, R.; Lin, Y.; Gao, J.; Meng, G. A high-performance ammonia-fueled solid oxide fuel cell. *J. Power Sources* **2006**, *161*, 95–98. [CrossRef]
210. Lin, Y.; Ran, R.; Guo, Y.; Zhou, W.; Cai, R.; Wang, J.; Shao, Z. Proton-conducting fuel cells operating on hydrogen, ammonia and hydrazine at intermediate temperatures. *Int. J. Hydrog. Energy* **2010**, *35*, 2637–2642. [CrossRef]
211. Zhang, L.; Yang, W. Direct ammonia solid oxide fuel cell based on thin proton-conducting electrolyte. *J. Power Sources* **2008**, *179*, 92–95. [CrossRef]
212. Xie, K.; Ma, Q.; Lin, B.; Jiang, Y.; Gao, J.; Liu, X.; Meng, G. An ammonia fuelled SOFC with a $BaCe_{0.9}Nd_{0.1}O_{3-\delta}$ thin electrolyte prepared with a suspension spray. *J. Power Sources* **2007**, *170*, 38–41. [CrossRef]

213. Khan, M.R.; Amin, M.; Rahman, M.; Akbar, F.; Ferdaus, K. Factors affecting the performance of double chamber microbial fuel cell for simultaneous wastewater treatment and power generation. *Pol. J. Chem. Technol.* **2013**, *15*, 7–11. [CrossRef]
214. Li, W.-W.; Yu, H.-Q.; He, Z. Towards sustainable wastewater treatment by using microbial fuel cells-centered technologies. *Energy Environ. Sci.* **2014**, *7*, 911–924. [CrossRef]
215. Yan, C.; Liu, L. Sn-doped V_2O_5 nanoparticles as catalyst for fast removal of ammonia in air via PEC and PEC-MFC. *Chem. Eng. J.* **2020**, *392*, 123738. [CrossRef]
216. Zacharakis-Jutz, G. Performance Characteristics of Ammonia Engines Using Direct Injection Strategies. 2013, p. 13032. Available online: https://lib.dr.iastate.edu/etd/13032 (accessed on 15 February 2021).
217. Gross, W.C.; Kong, S.-C. Performance characteristics of a compression-ignition engine using direct-injection ammonia–DME mixtures. *Fuel* **2013**, *103*, 1069–1079. [CrossRef]
218. Zamfirescu, C.; Dincer, I. Ammonia as a green fuel and hydrogen source for vehicular applications. *Fuel Process. Technol.* **2009**, *90*, 729–737. [CrossRef]
219. Mørch, C.S.; Bjerre, A.; Gøttrup, M.P.; Sorenson, S.C.; Schramm, J. Ammonia/hydrogen mixtures in an SI-engine: Engine performance and analysis of a proposed fuel system. *Fuel* **2011**, *90*, 854–864. [CrossRef]
220. Zamfirescu, C.; Dincer, I. Using ammonia as a sustainable fuel. *J. Power Sources* **2008**, *185*, 459–465. [CrossRef]
221. Brohi, E. Ammonia as Fuel for Internal Combustion Engines? *2014.* Available online: https://publications.lib.chalmers.se/records/fulltext/207145/207145.pdf (accessed on 23 December 2020).
222. Reiter, J.A.; Kong, S.-C. Diesel engine operation using ammonia as a carbon-free fuel. In *ASME 2010 Internal Combustion Engine Division Fall Technical Conference*; American Society of Mechanical Engineers Digital Collection: San Antonio, TX, USA, 2010.
223. Pearsall, J.T.; Garabedian, C.G. Combustion of anhydrous ammonia in diesel engines. *SAE Trans.* **1968**, 3213–3221.
224. Garabedian, G.C.; Johnson, J.H. *The Theory of Operation of an Ammonia Burning Internal Combustion Engine*; Army Tank-Automotive Center: Warren, MI, USA, 1966; pp. 333–348.
225. Cooper, J.; Crookes, R.; Mozafari, A.; Rose, J. Ammonia as a Fuel for the IC Engine. In Proceedings of the International Conference on Environmental Pollution, Zurich, Switzerland, 31 December 1991.
226. Reiter, J.A.; Kong, S.-C. Demonstration of compression-ignition engine combustion using ammonia in reducing greenhouse gas emissions. *Energy Fuels* **2008**, *22*, 2963–2971. [CrossRef]
227. Kong, S.-C. A study of natural gas/DME combustion in HCCI engines using CFD with detailed chemical kinetics. *Fuel* **2007**, *86*, 1483–1489. [CrossRef]
228. Ryu, K.; Zacharakis-Jutz, G.E.; Kong, S.-C. Effects of gaseous ammonia direct injection on performance characteristics of a spark-ignition engine. *Appl. Energy* **2014**, *116*, 206–215. [CrossRef]
229. Grannell, S.M.; Assanis, D.N.; Bohac, S.V.; Gillespie, D.E. The operating features of a stoichiometric, ammonia and gasoline dual fueled spark ignition engine. In *ASME 2006 International Mechanical Engineering Congress and Exposition*; American Society of Mechanical Engineers Digital Collection: New York, NY, USA, 2006; Available online: https://nh3fuelassociation.org/wp-content/uploads/2012/05/grannell_nh3.pdf (accessed on 18 January 2021).
230. Duynslaegher, C. *Experimental and Numerical Study of Ammonia Combustion*; University of Leuven: Leuven, Belgium, 2011; pp. 1–314. Available online: https://dial.uclouvain.be/pr/boreal/object/boreal:89103 (accessed on 12 January 2021).
231. Ezzat, M.; Dincer, I. Comparative assessments of two integrated systems with/without fuel cells utilizing liquefied ammonia as a fuel for vehicular applications. *Int. J. Hydrog. Energy* **2018**, *43*, 4597–4608. [CrossRef]
232. Hansson, J.; Fridell, E.; Brynolf, S. *On the Potential of Ammonia as Fuel for Shipping: A Synthesis of Knowledge*; Lighthouse Swedish Maritime Competence Centre: Göteborg, Sweden, 2020.
233. De Vries, N. *Safe and Effective Application of Ammonia as a Marine Fuel*; Delft University of Technology: Delft, The Netherland, 2019.
234. Laursen, R.S. Ship operation using LPG and ammonia as fuel on MAN B&W dual fuel ME-LGIP engines. In Proceedings of the 15th Annual NH3 Fuel Conference, Pittsburgh, PA, USA, 31 October–1 November 2018.
235. Shrestha, K.P.; Seidel, L.; Zeuch, T.; Mauss, F. Detailed kinetic mechanism for the oxidation of ammonia including the formation and reduction of nitrogen oxides. *Energy Fuels* **2018**, *32*, 10202–10217. [CrossRef]
236. Jojka, J.; Ślefarski, R. Dimensionally reduced modeling of nitric oxide formation for premixed methane-air flames with ammonia content. *Fuel* **2018**, *217*, 98–105. [CrossRef]
237. Nakamura, H.; Shindo, M. Effects of radiation heat loss on laminar premixed ammonia/air flames. *Proc. Combust. Inst.* **2019**, *37*, 1741–1748. [CrossRef]
238. Kobayashi, H.; Hayakawa, A.; Somarathne, K.K.A.; Okafor, E.C. Science and technology of ammonia combustion. *Proc. Combust. Inst.* **2019**, *37*, 109–133. [CrossRef]
239. Karabeyoglu, A.; Evans, B.; Stevens, J.; Cantwell, B.; Micheletti, D. Development of ammonia based fuels for environmentally friendly power generation. In Proceedings of the 10th International Energy Conversion Engineering Conference, Atlanta, GA, USA, 30 July–1 August 2012.
240. Iki, N.; Kurata, O.; Matsunuma, T.; Inoue, T.; Suzuki, M.; Tsujimura, T.; Furutani, H. Micro gas turbine operation with kerosene and ammonia. In Proceedings of the 11th annual NH3 Fuel Conference, Iowa, IA, USA, 21–24 September 2014.
241. Iki, N.; Kurata, O.; Matsunuma, T.; Inoue, T.; Suzuki, M.; Tsujimura, T.; Furutani, H. Micro gas turbine firing kerosene and ammonia. In *ASME Turbo Expo 2015: Turbine Technical Conference and Exposition*; American Society of Mechanical Engineers Digital Collection: Montreal, QC, Canada, 2015.

242. Hayakawa, A.; Goto, T.; Mimoto, R.; Arakawa, Y.; Kudo, T.; Kobayashi, H. Laminar burning velocity and Markstein length of ammonia/air premixed flames at various pressures. *Fuel* **2015**, *159*, 98–106. [CrossRef]
243. Okafor, E.C.; Naito, Y.; Colson, S.; Ichikawa, A.; Kudo, T.; Hayakawa, A.; Kobayashi, H. Experimental and numerical study of the laminar burning velocity of CH_4–NH_3–air premixed flames. *Combust. Flame* **2018**, *187*, 185–198. [CrossRef]
244. Ito, S.; Kato, S.; Saito, T.; Fujimori, T.; Kobayashi, H. Development of ammonia/natural gas dual fuel gas turbine combustor. In Proceedings of the NH3 Fuel Conference, Los Angeles, CA, USA, 18–21 September 2016.
245. Onishi, S.; Ito, S.; Uchida, M.; Kato, S.; Saito, T.; Fujimori, T.; Kobayashi, H. Methods for Low NOx Combustion in Ammonia/Natural Gas Dual Fuel Gas Turbine Combustor. In Proceedings of the 2017 AIChE Annual Meeting, AIChE, Minneapolis Convention Center, Minneapolis, MN, USA, 29 October–3 November 2017.
246. Ito, S.; Uchida, M.; Onishi, S.; Fujimor, T.; Kobayashi, T. Performance of Ammonia–Natural Gas Co-fired Gas Turbine for Power Generation. In Proceedings of the 15th Annu. NH3 Fuel Conference, Pittsburgh, PA, USA, 31 October–1 November 2018.